Classification of Teeth using Laser Induced Breakdown Spectroscopy

A Dissertation Submitted

To

Sikkim University

In Partial Fulfillment of the Requirement for the
Degree of Master of Philosophy

By
Puja Pradhan
Department Of Physics
School Of Physical Science

August 2021

**This Thesis is Dedicated to My Grandmother,
Late Narbada Pradhan**

Declaration

I, Puja Pradhan, declare that the thesis entitled **"Classification of Teeth using Laser Induced Breakdown Spectroscopy"** submitted in partial fulfilment of the requirement for the degree of **"Masters of Philosophy in Physics"** to Sikkim University is the compilation of my original work. The content of the thesis is based on the experiments and analysis that are performed by me. Information that is derived from the literature is duly acknowledged in the text and is listed in the provided references. The thesis has not been submitted for any other degree or diploma.

Puja Pradhan

(Puja Pradhan)

Roll No.: 18MPPY01

Regn. No.: 18/M.Phil/PHY/01

Date: 9.8.21

Recommended that this M.Phil thesis to be placed before the Examiners for evaluation.

(Dr. Ajay Tripathi)

Supervisor

Date: 9.8.21

सिक्किम विश्वविद्यालय
SIKKIM UNIVERSITY

(भारत के संसद के अधिनियम द्वारा वर्ष 2007 में स्थापित और नैक (एनएएसी) द्वारा वर्ष 2015 में प्रत्यायित केंद्रीय विश्वविद्यालय)
(A central university established by an Act of Parliament of India in 2007 and accredited by NAAC in 2015)

Certificate

This is to certify that the M.Phil thesis entitled **"Classification of Teeth using Laser Induced Breakdown Spectroscopy"** submitted to Sikkim University in partial fulfilment of the requirement for the degree of **"Masters of Philosophy in Physics"** presents the results of genuine research work performed by **Miss. Puja Pradhan** under my guidance and supervision. The results are original and are not been submitted anywhere for any other degree or diploma.

All the assistance and help required during the course of investigation has been duly acknowledge by her.

(Dr. Ajay Tripathi)
Supervisor
Department of Physics
School of Physical Sciences
Sikkim University

Place: Gangtok, Sikkim

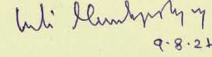Date: 9.8.21

सिक्किम विश्वविद्यालय
SIKKIM UNIVERSITY

(भारत के संसद के अधिनियम द्वारा वर्ष 2007 में स्थापित और नैक (एनएएसी) द्वारा वर्ष 2015 में प्रत्यायित केंद्रीय विश्वविद्यालय)
(A central university established by an Act of Parliament of India in 2007 and accredited by NAAC in 2015)

Certificate

This is to certify that the M.Phil thesis entitled **"Classification of Teeth using Laser Induced Breakdown Spectroscopy"** submitted to Sikkim University in partial fulfilment of the requirement for the degree of **"Masters of Philosophy in Physics"** contents the work carried out by **Miss. Puja Pradhan** for the award of M.Phil degree in Physics, Department of Physics, Sikkim University, Gangtok, Sikkim. The results are original and are not been submitted anywhere for any other degree or diploma.

It is recommended to place the M.Phil thesis before the Examiner for evaluation.

9·8·21

Head of the Department

(Dr. Subir Mukhopadhyay)

Associate Professor

Department of Physics

School of Physical Sciences

Sikkim University

Gangtok-737102

अध्यक्ष
Head
भौतिकी विभाग
Department of Physics
सिक्किम विश्वविद्यालय
Sikkim University

Place Gangtok, Sikkim

Date: 9. 8. 21

PLAGIARISM CHECK CERTIFICATE

This is to certify that plagiarism check has been carried out for the following M. Phil thesis with the help of OURIGINAL software and the results is within the permissible limit of 2% as per the norms of Sikkim University.

"Classification of Teeth using Laser Induced Breakdown Spectroscopy"

Submitted by **Puja Pradhan** under the supervision of **Dr. Ajay Tripathi** of the Department of Physics, School of Physical science.

Puja Pradhan
10.8.21
(Puja Pradhan)
Signature of the candidate

9/08/14
(Dr. Ajay Tripathi)
Countersigned by M. Phil supervisor.

10/08/2021
Vetted By Librarian

पुस्तकालयाध्यक्ष
Librarian
केन्द्रीय पुस्तकालय Central Library
सिक्किम विश्वविद्यालय
Sikkim University

Acknowledgement

Abstract

The project is based on the study of human teeth samples of various age groups (5-60 years) and classifying them using laser-induced breakdown spectroscopy (LIBS) coupled with multivariate analysis. The hardness of calcified tissue varies with the aging process due to various environmental conditions, dental infections, mineral deficiencies, and many more. Therefore, our objective here is to estimate the hardness of human teeth samples for various age groups and perform age-wise classification, considering hardness as a varying factor. A human tooth is calcified, crystalline tissue composed of mineralized hydroxyapatite, $Ca_{10}(PO_4)_6(OH_2)$ and consists of enamel(96% of mineralized inorganic material and 4% organic material), dentin(70% mineralized inorganic material, 20% organic material and 10% water) and cementum(65% mineralized inorganic material 23% organic mineral and 12% water) sections. Therefore, Ca, P, O, and H are the major elements of a human tooth along with the presence of trace elements like Cl, F, Na, K, Sr, Mg, Mn, Cu, Zn, Pb. The hardness of a calcified tissue can be estimated by measuring the ratio of ionic to neutral emission lines of Ca and Mg. LIBS is the most robust spectroscopic method for performing elemental and ratiometric analysis of dental samples. Here, we study the enamel and cementum sections of the teeth separately as the hardness is found to vary differently between these two sections. To examine which section is better suited to classifying the teeth samples, three different multivariate approaches were taken. First, we establish a quantitative picture of the variation of hardness in the two sections independently with a histogram plot (1D classification). The variation in ratio values of Ca and Mg estimated from the 1D classification is further defined and supported using the 2D classification. Further, the variation in the LIBS spectra obtained for six different age groups for each of the enamel and cementum sections is classified with multidimensional PCA analysis.
By using LIBS, we have detected the presence of Ca, P, H, and O as the major elements. In addition, we also detected Mg, Sr, Na, and Zn as trace elements. By evaluating the ratios of $\frac{CaII(422.7nm)}{CaI(442.67nm)}$, $\frac{CaII(500.14nm)}{CaI(442.67nm)}$, $\frac{MgII(526.443nm)}{MgI(517.16nm)}$, for both sections, we have investigated the variation in the hardness with age.

The variation in the evaluated ratio was prominent in cementum as compared to enamel. Our results show that cementum is better suited to performing classification of human teeth as variation in hardness and intensity are clearly observed. Further, we verified this with various multivariate analysis like 1D, 2D and PCA. Our findings support the robustness of LIBS to perform the elemental analysis of calcified biological samples and the importance of the laser in the fields of odontology, archeology, and forensic science.

Presentation and Publication

Presentation

P.Pradhan, A. Tripathi, and R. Rawat, "Classification of teeth using Laser induced breakdown spectroscopy", International Seminar on Correlative Advancement on Analytical and Applied Physics. October 21-22 2019. Department of Physics in collaboration with IQAC St. Joseph's College, Northpoint, Darjeeling. **(ORAL presentaion)**

Publication

"Classification of human teeth using laser induced breakdown spectroscopy", P.Pradhan, A. Tripathi, and R. Rawat.**(Under progress)**

Contents

List of Figures

List of Tables

Chapter 1

Introduction

1.1 Introduction

Laser-induced breakdown spectroscopy

Laser-induced breakdown spectroscopy (LIBS) is a rapidly growing atomic emission spectroscopic technique in the field of elemental analysis. It comprises a high-power pulsed laser of short duration which is targeted at the study material or sample. A laser-induced plasma plume is formed, which bears the fingerprints of elements present in the sample. Using emission spectra obtained from the plasma, a range of elements present in the sample can be detected and studied [1, 2, 3]. The advantages that are associated with the technique are: It effectively reduces the time for sample preparation, and is versatile as a range of samples (solids, liquids, gases, and so on) can be analyzed with ease. The amount of sample does not influence the outcome of analysis and is a robust and rapid process. Therefore, with these benefits of LIBS, the growth in qualitative and quantitative elemental analysis of diverse samples is extremely fascinating [4, 5, 6]. The features of the technique,

such as laser source, regulation of pulse energy and duration, resolution of spectrometer, optical setup for collection of emission lines, modification in plasma conditions, have improved since the day its first useful application was achieved [2, 4]. At present, the desired amount of data can be generated with LIBS, which allows to study the material extensively with accuracy and precision. The application of LIBS is not limited to laboratory examination of the sample. Rather, real-time analysis of samples at site through portable LIBS is also possible. In-vivo, in-vitro analysis of biomedical samples, space exploration with remote LIBS, and underwater examination of samples are made possible with LIBS. The other standard atomic emission spectroscopic techniques, such as atomic absorption spectroscopy (AAS), atomic emission spectroscopy (AES), inductively coupled plasma mass spectroscopy (ICP-MS) and x-ray fluorescence (XRF), are as efficient as LIBS. The disadvantages of these methods are related to strict sample preparation protocols, therefore all kinds of samples can not be analysed. The quantity of sample and its homogeneity play a major role in the outcome and detection of lighter elements such as C, H, O, N is difficult with these techniques. In the matter of sensitivity and accuracy, few of these techniques have greater advantages over LIBS. This discrepancy can be resolved to some extent by introducing the double-pulsed LIBS (DP-LIBS) and multi-pulsed LIBS (MP-LIBS) [14]-[24]. With these advancements, LIBS is very useful in space exploration, in the elemental analysis of environmental, industrial, archeological, geological, nanomaterial, and forensic materials. Higher energy materials, plant and animal physiology, human biology, and many more.

Principal component analysis (PCA)

With the ability of LIBS to generate thousands of variables and huge spectral data, it is crucial to handle the exhaustive data adequately. There arises the need to introduce sophisticated algorithms for effective and fast processing of data. Therefore, in this scenario, multivariate analysis efficiently handles the LIBS data [11]. Multivariate methods are of two kinds, namely supervised and unsupervised pattern recognition methods. In the former method, a model is constructed based on known samples and is further used to predict unknown samples as well. Partial least square discriminant analysis (PLS-DA), linear discriminant analysis (LDA), k-nearest neighbor (kNN), artificial neural networks (ANN), and soft independent modelling class analog (SIMCA) fall under this method. The unsupervised method is an initial step of data analysis used for dimension reduction and pattern formation of the dataset by maintaining the originality of the data. Principal component analysis (PCA), cluster analysis such as K-mean and hierarchical cluster analysis (HCA) are unsupervised pattern recognition methods for classification. The most widely used multivariate analysis in laser physics (LIBS, NIR, FTIR, etc) is PCA, for classification of samples and as a preliminary step for further analysis [11]. PCA was first planned in statistics by Pearson and was brought to its present state by Hotelling. In PCA, the dataset is expressed as a linear combination of a few linearly independent variables or principal components (PCs). These PCs can explain the maximum variables present in the dataset. The multidimensional data is reduced to the subspace defined by new PCs, making the interpretation of data easier. An additional

set of basis will eliminate noise and bring out the actual pattern of the set. By correlating the properties of samples to the patterns, classification of the samples can be performed. To perform PCA, the sample matrix should be covariance or correlated, and multiple variables must be present. Linearity among the variables must be maintained and should be correlated. Each value needs to follow a normal distribution and must be free from outliers. The two important aspects of PCA are the loading plot and the score plot. The loading is linear coefficients of the inverse relation of linear combinations. It helps to understand the dependence of variables on PCs and establish a correlation between them. The score plot is the projection of original sample data onto the new PCs and is the actual output of PCA [7]-[11].

We come to know that in the present era, LIBS with multivariate analysis is the fastest growing technique in the laser community and spectrochemical analysis of samples. The technique of coupling LIBS with multivariate analysis is found to be very useful in the fields of biomedical and forensic science. Identification of various pathological diseases, malignant tissue, classification of organs, and pathological bacteria is made possible with LIBS and a multivariate technique. The study of calcified tissue is important as they are stable compounds and can retain biological information for a long duration. The identification of principal elements along with trace elements present in the calcified tissues is possible with LIBS. Along with this, changes in the concentration of principal elements due to environmental, habitation conditions, etc. can also be observed with LIBS. By identifying normal and pathological conditions, variation in elements with aging or environmental factors, biomedical and forensic sciences can be better understood with LIBS

in combination with chemometrics.

In this project, we aim to study the human teeth samples of various age groups. A human tooth is one of the hardest calcified tissue, crystalline in nature, and is composed of mineralized compound hydroxyapatite $Ca_{10}(PO_4)_6$ (OH_2). Therefore, Ca and P are major elements found in a human tooth along with the presence of trace elements like Cl, F, Na, K, Sr, Mg, Mn, Cu, Zn, Pb which are incorporated due to various environmental conditions during teeth formation. The human tooth is divided into three regions viz., enamel, and dentin which forms the crown region, and cementum forms the root. Enamel is composed of 96% of mineralized inorganic material and 4% organic material and is the hardest and most mineralized section. Dentin consist of the pulp and is made of 70% mineralized inorganic material, 20% organic material and 10% water. Cementum contains 65% mineralized inorganic material, 23% organic mineral and 12% water [5, 103, 104]. The elements that are investigated as shreds of evidence for forensic information and examined for human pathological conditions are present in human teeth. Therefore, it is easy to access and laser science is one of the most extensively applied techniques in dentistry. Also, the hardness of a calcified tissue can be estimated by the ratio of intensities for the ionic and atomic lines of Ca and Mg. $\frac{CaII}{CaI}$ and $\frac{MgII}{MgI}$ are proportional to the hardness of tissue. Therefore, our motive here is to analyze the hardness of teeth samples for the enamel and cementum section by utilizing these ratios. Studies show that hardness varies between the enamel and cementum sections and remains unchanged for dentin [12]. The variation of these ratio values is observed for all the age groups for both sections. Age classification based on these values is analyzed

with histogram plot as 1D classification and with 2D classification. Lastly, PCA is applied for age-wise classification of samples considering the entire LIBS spectra for the enamel and cementum section. A comparative study was performed to check which section is better suited for the classification of teeth samples with varying ages.

1.2 Objective

There are three main objectives of this work which are as follows :

1. To perform elemental analysis of human teeth samples with LIBS for the age group between 5-60 years. The two sections of the teeth samples, viz., enamel and cementum part of the samples are examined.

2. The next motive is to estimate the hardness of these two sections by taking the intensity ratio of ionic to neutral lines of Ca and Mg. These values are obtained for all the age groups and the classification of teeth samples based on varying hardness with aging is obtained with 1D and 2D classification.

3. Finally PCA is done on the entire LIBS spectra for both the section and classification of teeth samples with ascending age is estimated.

The application of LIBS with PCA to study the hardest section among enamel, dentin, and cementum of a human tooth is reported in the literature by Pathak, et al, [12]. They have evaluated the hardness of teeth samples by observing the ratio intensities for the ionic to atomic lines of Ca and Mg, $\frac{CaII}{CaI}$ and $\frac{MgII}{MgI}$. The results show enamel to be the hardest section and hardness varies for the enamel and cementum section with age but remains the same for dentin. The study is limited to the application of PCA to identify the hardest section of the sample [12]. The variation of the hardness and corresponding changes in the LIBS spectra with age remain untouched. Therefore, our aim here is to classify human teeth samples with varying ages on the basis of hardness and the variation in the LIBS spectra

by using various multivariate techniques. This study shows which of the two sections of enamel and cementum can be better suited to classifying human teeth samples with age.

1.3 Review of Literature

1.3.1 Introduction to laser induced-breakdown spectroscopy (LIBS)

Based on the Albert Einstein theory of stimulated emission, laser-induced breakdown spectroscopy (LIBS) marks its development with the invention of the pulsed ruby laser in the year 1960. The first useful laser-induced plasma produced for spectrochemical analysis of surfaces in the year 1963 led to the birth of LIBS. Over the years, there has been a significant development in this technique and has created an opportunity to explore a wide range of samples [5, 12]. LIBS is a technique based on atomic emission spectroscopy. The process involves the excitation of atoms in the ground state by the application of an external energy source. The atoms in an excited state spontaneously emit radiation to reach the lower or ground state. The emission intensity while returning to the lower state is directly proportional to the concentration of atoms in the ground state [1]. Based on this principle, in LIBS, a high-power pulsed laser of short duration is targeted at the surface of a study material (solid, liquid, gas). When the laser power irradiance exceeds the breakdown threshold, the illuminated section of the sample gets ablated. The process is accompanied by phenomena like local heating, melting, and intense evaporation. The evaporated material expands and, because of its high temperature, it forms a plasma plume above the surface of a sample. Plasma is the local assembly of atoms, ions, molecules, free electrons, neutral and excited species present in a sample. Collection of emissions from plasma while it is cooling

down, gives the idea about the content of the sample [1, 2, 3, 4, 5].

Due to its monochromatic, directionality, generation of high-power pulsed beam, and coherence properties, the laser has gained importance in modern spectroscopy. The Q-switched Neodymium-doped Yttrium Aluminum Garnet (Nd: YAG) is a laser system used in LIBS because it has properties such as higher repetition rates, better pulse-to-pulse repeatability, improved optical-beam characteristics, durability, reduced size, and better energy efficiency. Generally, it is operated at the fundamental wavelength of 1064 nm, although other wavelengths (532 nm, 355 nm, and 266 nm) can be generated. The laser operating conditions such as wavelength, pulse duration, and pulse energy are the factors that affect laser ablation and laser-induced plasma formation. [2, 4, 5].

We briefly discuss the working function of a few other widely used atomic spectroscopy techniques in table 1.1 and the disadvantages related to them. These disadvantages are overcomed with LIBS, which makes it a convenient technique compared to other methods.

Table 1.1: Comparision between the atomic spectroscopy techniques other than LIBS.

Methods	Working Principals	Disadvantages
AAS	Absorbs ultraviolet/ visible light to measure the concentration of metallic elements in the gas phase. The flame or graphite furnance dries, ashes and vaporizes the sample to produce free analyte atoms[1, 14].	The samples are dissolved hence information about the concentration and spatial location is destroyed. Only single element can be analysed at a time and detection of organic components such as C, H, N, O is difficult [15, 16].
AES	The concentration of analyte atoms are determined with optical emission. The desolvated, vaporized and atomized atoms are excited into higher energy levels with high-temperature atomization source. It emits radiation while decaying to lower levels [17].	Simultaneous detection of elements are possible, but the spectra are narrow and congested. Therefore, it requires high-resolution spectrometer[14].
LA-ICP-MS	The laser ablated samples are vapourised and ionized in the ICP. Based on the production of ions in ICP elements are detected through their mass to charge ratio. Precise identification of trace elements is possible for sample concentration less than 1 ppm [18, 19].	In terms of sensitivity and precision LA-ICP-MS is a better techinique but the results highly depends in the method of sample preparation [20, 21].
XRF	Targeted X-rays on finely powdered and homogeneous sample, knocks out electrons from inner orbitals of atom. A photon with characteristics of particular element is ejected as electrons from outer orbitals falls in to fill the void.	Condition for detection are weight >1 g, $Z \geq 12$. The spatial resolution is low and interference can mask identification of elements. Portable field XRF has a low peneration[14, 12, 5, 22, 23, 24].

1.3.2 Importance of LIBS with multivariate analysis.

In recent years, a dynamic advancement has been recorded in LIBS, with the improved repetition rate, resolution, and sensitivity of the laser and detection unit. Henceforth, a desired number of spectra can be generated with LIBS to accurately examine the composition of a sample. With an increase in the repetition rate of a laser, the number of measurements is high and the corresponding variables for each measurement are also large.Therefore, to characterize the sample by processing a large dataset requires the application of multivariate data analysis. The purpose of using multivariate analysis is to determine all the variations in the data matrix and to find the relationships between the samples and variables in a given data set and convert them into new latent variables. The multivariate algorithm efficiently classifies the sample matrix based on its spectral features. The advantage of using multivariate analysis is due to the efficient reduction of multi-dimensional variables into lower dimensions by preserving the originality of data. The detection of outliers helps to identify the pattern present in the sample, which is helpful for sample classification [10] [25]. Of the various multivariate analysis methods, the most widely used in the LIBS community is PCA. The main motive of PCA is to extract important data from the sample matrix and compress the data set, keeping only important features. The new information is expressed as a set of new orthogonal variables called principal components, which simplifies the description of a dataset. It helps us to observe the structure of measurements and variables, which eventually helps in sample classification [9]. The mathematical details of PCA will be

discussed in chapter 2. Here we briefly review the application of LIBS with PCA in various fields.

Pharmaceuticals, Medicinal herbs.

All pharmaceuticals are composed of organic active substances known as active pharmaceutical ingredients (API) and excipients, which consist of various inorganic elements present as additives or impurities. Therefore, LIBS is applicable here as it can detect both organic and inorganic elements at once. A study was conducted by Myakalwar et al.,[26] to investigate the effectiveness of LIBS for monitoring commercial pharmaceutical tablets based on their compositions and for further investigation using PCA and SIMCA. PCA has been employed to classify Brufen (coated and uncoated), Glucosamine (coated and uncoated), Paracetamol, and Vitamin C. A fair classification of samples has been observed and their results conclude that PCA can identify the primary elements existing in the sample composition, which helps in distinguishing the various samples [26]. P.K. Tiwari, et al., studied various brands of Type 2 diabetes drug tablets containing voglibose ($C_{10}H_{21}NO_7$) as an API having dose strengths of 0.2 and 0.3 mg with LIBS and processed the data using PCA and PLSR for classifying and also developing the calibration models of drug samples. For this, the LIBS spectrum was recorded from five uncoated samples in argon and air medium. Although the same elemental composition was found in all the samples, PCA has given distinguishable clusters for all the samples in both air and argon medium [27]. The same group has studied the composition and classification of pain-relief drugs in the air and argon atmosphere. The elemental analysis from the LIBS shows

the presence of C, Hα, O, N, Na, Mg, Ca, Si, along with the presence of CN
and C_2 bands. A satisfactory classification of these samples has been per-
formed with PCA showing its ability to discriminate/classify a huge number
of drugs having nearly similar or different compositions [28]. The work of
Doucet et al., points out the capability of LIBS to detect molecular bands
of CN, CH, C_2, atomic lines of C, H, Mg, and ionic lines of Ca. With the
detection of these elements, one can predict all the ingredients present in
a complex matrix of a pharmaceutical formulation. Therefore, using LIBS
coupled with chemometric tools, a complete study of pharmaceutical tablets
can be done both qualitatively and quantitatively [29]. LIBS has been ap-
plied to study multielement tablets and the results obtained agree with those
obtained from the ICP OES technique. Henceforth, LIBS could be a suitable
alternative to the current wet chemistry method [30].

In recent studies, LIBS has been efficiently used to perform the elemental
analysis of medicinal plants of various kinds. The application of multivariate
analysis to classify the herbs from different provinces has gained importance.
Here we highlight a few applications of LIBS with multivariate analysis in
this field. J.Wang et al., has investigated three kinds of Chinese medicinal
herbs i.e., *angelica pubescens*, *Ligusticum wallichii* and *Codonopsis pilosula*
taking its root section. The effectiveness of Chinese medicinal herbs is be-
lieved to depend on factors like origin, collection time, and processing meth-
ods. Therefore, qualitative and quantitative characterization of the herbs is
required. The samples were taken from different places and have been clas-
sified with PCA and back-propagation artificial neural network (BP-ANN).
Incorporating the NIST database with LIBS, identification of elements like

K, Ca, Na, Mg, Al, Fe, Li, Ba, Si, and C were possible. PCA has successfully classified the roots of *angelica pubescens* originating from different places. For classification of the other two samples, PCA has been coupled with BP-ANN [31]. The same group has performed the elemental analysis of Puer tea leaves, which is a kind of fermented dark tea, with LIBS. Here quantitative analysis of Pb which is a toxic heavy metal is done by three methods: external standard method, internal standard method, and multiple linear regression method. The study confirms that LIBS combined with multiple linear regression method is a favorable method for analyzing the concentration of Pb in Puer tea leaves [32]. Also, the different kinds of tea samples has been analyzed with LIBS and classified using discriminant analysis(DA). The spectral lines of Mg, Mn, Ca, Al, Fe, K, CN, and C_2 were used from the LIBS spectra for evaluation of the samples. Out of 300 samples, 286 samples were identified correctly with the average identification rate of 95.33% [33]. The study of *Artemisia annua*, a traditional Chinese herb has been done with LIBS using wavelengths of 532 nm and 1064 nm. Its purpose was to investigate the influence of laser wavelengths on the detection of metals in the elemental analysis of the herb [34]. The work of D.K Tripathi et al., investigates the micro-and macro-elements distribution in the leaves of four *Ocimum* species viz. *Ocimum basilicum*, *Ocimum sanctum*, *Ocimum gratissimum* and *Ocimum americanum*. Analysis of the sample was done with LIBS and ICP-AES which confirms the presence of K, Na, Ca, Mg, Si, C, H, O, N, with Ca in abundance. The lighter elements like C, H, O, N were not detected by the latter method. PCA formed separate clusters for all four species of *Ocimum*, proving that there is a difference in mineral accumulation

and its distribution among them [35]. Similarly, X.Liu et al., has performed the elemental analysis of *Blumea balsamifera*, collected from different origins with LIBS and employed PCA and PLS-DA to classify them. LIBS spectra mark the presence of Ca, K, Na, Mg, Al, H, N, and O. Their study shows that better classification is obtained with PLS-DA [36].

Environmental analysis

Due to the capability of LIBS to perform remote and on-site investigation of a sample, it is finding a wide application in environmental monitoring of toxic water samples, soil contamination, and rocks. The work of G. Kim and his group highlights the application of LIBS to perform elemental analysis of soil contaminated with heavy metals or oil and classify them using PCA and PLS-DA. The emission lines of C, Ca, Cd, Cr, Cu, Fe, Mg, Al, Mn, Nb, Pb, Si, Sr, Ti, V, and Zn were observed in LIBS spectra. The concentration of Cu, Pb, and Zn were found to be higher in the contaminated soil. The concentration of Al, C, Cu, Fe, Pb, Si, and Zn were found to decrease with the increase in water content of the soil. PCA with two principal components (PC1 and PC2) formed a separate cluster for the soil contaminated with heavy metals and overlapping was observed between the clean soil and oil-contaminated soil. By including the third principal component (PC3), classification of all three samples was possible [37]. S.Chatterjee and the group have investigated the soil from the Manuguru geothermal area, located in the Telangana state, with LIBS and PCA. The soil samples were collected from spots near the thermal discharge and away from it. The chemical analysis and LIBS show the abundance of trace elements like Li, Rb, Cs,

B, Sb, Cu, Pb, Mn, Co, rare earth elements; Sc, Ce, Eu, Tb, and transition metals; Hf, Ta, in the soil samples collected near the thermal discharge. PCA when run through the entire LIBS spectra showed the clustering of samples near the thermal site and away from it. Therefore, the concept of an arbitrary parameter named PCA coefficient threshold (T^c) was introduced to the maximum Cartesian distance in the loading plot. This allows selecting only the important wavelength region to perform the classification. By applying this criterion to PCA, better classification was obtained. The chemical data showed a distinct cluster for both the regions, classifying the sample with an accuracy of 85% [38]. Similarly, LIBS with PCA and PCR has been employed to investigate soil bacteria from un-mined bauxite soil and historically mined bauxite soils. Femtosecond LIBS has been employed to study isolated bacteria and mark the emission lines of Na, Mg, K, Zn, Ca. PCA has been applied to classify the bacteria found at individual sites. This result shows the efficiency of LIBS in identifying the chemical composition of bacteria and accordingly classifying them [39].

The study by J.B Servine and his group focuses on the remote identification of rocks by LIBS under Martian conditions. This is the laboratory investigation of ChemCam before it was equipped for the Mars Science Laboratory (MSL) in 2007. ChemCam (Chemistry and Camera) is NASAs 2011 MSL rover named Curiosity, designed to evaluate whether the Martian environment is capable of supporting microbial life. It consists of two standoff sensing instruments: LIBS and a Remote Micro-Imager (RMI), mounted on the rover body to perform elemental analysis at a distance of 2 to 9 m. LIBS performs the elemental analysis while RMI places the LIBS analyses in the

geomorphological context [40]. Here, six different kinds of rocks, viz. Gabbro, Limestone, Obsidian, Basalt, Trachyte, and Trachy-andesite, have been examined with LIBS and have been classified using three different multivariate methods, i.e., PCA, SIMCA, and PLS-DA. With PCA, four of the rock samples could be classified except for basalt and gabbro as they possess similar spectral features. The drawback of PCA is that automatic predictions can not be performed. Therefore, SMICA has advantages for remote identification of Martian rocks as it avoids misclassification even if most of the spectra remain unidentified [40]. A similar study has been conducted to examine igneous and highly-metamorphosed rock samples with the application of PLS and PCA, mainly to create a calibration system for ChemCam [41]. Similarly, the work of Lanza and his group examines the weathered rocks with LIBS in a martian atmosphere to improve interpretations of ChemCam rock analyses on Mars as the composition of rocks changes with the addition and removal of substances. Rock coating and rinds are two kinds of weathering processes observed in situ on the Martian surface. Therefore, four naturally weathered Basaltic rocks were taken as the sample and were examined in both interior (fresh) and exterior (weathered) environments. O, Si, Fe, Al, Mg, Ca, Na, and K are the major elements found in all the samples. With the help of PCA, the variety of elements from the exterior to the interior interior region has been observed and classification has been performed [42]. A significant application of LIBS with PCA was found in the investigation of mineral ores, as shown in the work of P. Pozka, where they studied igneous rocks from various provinces. The study is divided into two parts: In system 1, a high energy Nd: YAG laser of 1064 nm wavelength was used to irradiate

the sample, and in system 2, a diode-pumped solid-state (DPSS) laser was used. The outliers for PCA were more clear in system 2 and the classification was more distinct [43]. Similarly, the application of LIBS with PCA was found in the analysis of geomaterial classification and mineral ores [44, 45]. Liquid analysis by LIBS is difficult due to various factors. The free surface of the liquid and the presence of microbubbles and particles hinder the results. The high density and cooling effects of a liquid sample cause quenching of laser-induced plasma, therefore the plasma has a lower temperature, lower emission intensities, shorter lifetimes, and smaller maximum dimensions. A double-pulsed LIBS is widely applied to study liquid samples, where the first laser pulse creates a cavitation bubble and the second pulse, which is slightly time-delayed, excites the plasma within them. This aids in the production of more intense and narrow spectral lines. The other method is to analyze the liquid sample in bulk form where the laser is focused on the free surface or within some depth of the liquid. The first analysis of bulk aqueous liquid was reported by Cremers et al., using a single and double pulsed laser [4, 46]. Here we would like to cite some applications of LIBS in liquid analysis. LIBS has been used to detect Cr as a toxic metal in waste released from a refuse incineration power plant near Poyang Lake, China. The experiment was carried out with a single-pulsed laser and the optimization of laser pulse energy, signal delay, and repetition rate improved the intensity of the spectra. The obtained results have been compared with the AAS technique and a standard deviation of 8.5% is recorded [47]. To detect Pb and Cr in an aqueous solution with LIBS, an ordinary printing paper is used as a liquid absorber which is immersed in $Pb(NO_3)_2$ and $Cr(NO_3)_3$. This method enhances the

sensitivity and limit of detection (LOD) of metal ions in solution for LIBS. The reproducibility of line intensity is improved with a relative standard deviation of $\sim 4\%$ [48]. Similarly, the presence of arsenic (As) in underground water with LIBS has been tested using zinc oxide (ZnO). This allows us to measure the concentration of as low as 1 ppm [49].

Food and industrial application

The application of LIBS in the food industry for the analysis of milk, bakery products, tea, vegetable oils, water, cereals, flour, potatoes, palm dates, and different types of meat is increasing rapidly. Also, its application is widely found in the analysis of alloys, plastics, waste, ceramics, glasses, and nuclear plants [50, 51]. LIBS has been employed to classify the different natures of fertilizers using multivariate analysis like PCA and PLSR. Phosphate rocks and organomineral fertilizers of different origins and composition are studied with single and double pulsed LIBS. The presence of P, Ca, and Fe has been verified with LIBS and the concentration is measured with ICP-OES. PCA is performed on the raw as well as on normalized spectra which successfully classifies the phosphate and organomineral fertilizers [52]. The study of genetically modified (GM) and non-GM maize samples was analyzed with LIBS in combination with PCA, PLS-DA, SIMCA, and ELM. The mineral elements detected were Mg, Al, Ca, Fe, K, Ti, and also the molecular bands of CN were identified. The concentration of minerals in GM maize samples was less than in non-GM maize. The PCA results could classify the samples, where the variables mainly remained dependent on PC1. According to the PCA results, 30 main emission lines were taken to further analyze them

with PLS-DA, SIMCA, and ELM [53]. The applicability of LIBS is also found in quality control, traceability, and detection of adulteration in milk. The combination of PCA and neural networks (NN) was used to achieve classification of pure and mixed milk samples. Also, the quantification of melamine in toddler powder milk samples was studied by NN [54]. Similarly, qualitative classification between pure meat and offal samples and their adulteration is quantitatively studied with LIBS and PCA. Offal samples consist of the kidney, liver, heart, lungs, and spleen of beef. Therefore, LIBS analysis of all these parts was taken, which marks the presence of Na, Fe, K, Mg, and Ca in different concentrations for different parts. PCA was successfully used to classify among the different types of offal samples and PLS was employed to study the adulteration of offal mixtures [55]. The analysis of animal fat extracted from different animals is done with LIBS. The samples were frozen using the freezer method and liquid nitrogen (LN_2), and have shown enhancement in the amplitude of LIBS spectra. PCA was successfully applied to classify the samples frozen with the above mentioned two techniques, though extracted from the same sample. Also, discrimination between samples extracted from different species under the two freezing processes is analyzed with PCA, showing (LN_2) as a better method of freezing [56].

The application of LIBS is equally important in the classification of alloys. The time-resolved LIBS is employed to study materials made of carbon steel, stainless steel, high-temperature steel, mild steel, zirconium alloy, nickel alloy, brass, copper, and aluminium [58]. The multivariate analysis employed are PCA, cluster analysis, multiple discriminant method, and the spectral

matching method. The classification between samples having similar elemental composition could not be classified with PCA but provides a spectral identification for general elements. The multiple discrimination method brings more accuracy in the classification of samples [58]. The analysis and classification of coal ash are studied with LIBS in combination with PCA and independent component analysis-wavelet neural network (ICA-WNN), as it is useful in the management of metallurgical waste. The identification of coal ash with WNN requires the formation of a training model. The optimization of input variables, pre-processing method, model parameters, and validation of the training model are required. Therefore, PCA with Mahalanobis distance (MD) was first employed to identify the abnormal spectra in LIBS to optimize the training set. The refined input obtained with PCA and ICA was used to classify the samples with WNN [59]. The practice of remote detection using LIBS has increased the possibility of its application in a hostile environment. A study explores the ability of LIBS to discriminate between pre-irradiated nuclear Pile Grade A (PGA) graphite moderator rods and domestic lump wood charcoal, which causes nuclear waste. The emission lines of C(I), C_2, Ca(II), Ca(I), CN, Fe, Mg, Na re recorded for charcoal lump. PCA could classify between groups of graphite moderators and charcoal lumps with different pulse energies. Further clustering methods, molecular and atomic discrimination methods are employed to improve the classification [60].

Archeology and forensic

The properties of LIBS to perform rapid elemental analysis of samples at the site with minimal destruction and with depth-profile analysis have attracted people to investigate archeological sites with its application. Several historical artifacts, which include ancient buildings, paintwork, coins, and ceramics, are explored by LIBS [61]. The historical buildings were characterized according to the building materials mined from different quarries around Spain with LIBS and XRF. The samples were divided into two groups. The first consisted of samples of known origin and the second group consisted of samples of unknown origin. A relatively small number of major and trace elements are detected with LIBS, which are Mn, Cr, Pb, Cu, Sr, Ti, Si, Mg, Fe, Ca. XRF measures a large set of elements such as As, Ba, Cl, Co, Cr, Cu, Ga, Hf, La, Mo, Nb, Nd, Ni, Pb, Rb, Sc, Sm, Sr, Ta, Th, Tl, V, U, W, Y, Yb, Zn, and Zr. Therefore, the latter method is applied here to resolve incomplete classification based on LIBS data. LDA is employed on the XRF data to classify the materials, which could discriminate against only four kinds of building materials. PCA was applied to LIBS data with the first two principal components. The first group of samples could classify two kinds of materials, but the rest remained clustered together. This was resolved by introducing successive principal components which showed scattered data, which is attributed to the intrinsic heterogeneous nature of study samples. The further classification is carried out with SIMCA to bring clarity to the classification [62]. Archaeological coins obtained from the excavations in Kausambi, Uttar Pradesh, India are studied with LIBS. Five coins belonging

to different dynasties have been investigated. The LIBS spectra of coins show the emission lines of Ag, Cu, Ca, Si, Fe, Mg, and Sn. PCA could successfully classify the samples, forming five separate clusters, proving that it can classify samples with different compositions as well as of different matrices. Also, the loading plot establishes the correlation among all the elements detected and their dependence on the principal components [63]. The application of LIBS is reported for the analysis of ancient ceramics of different origins. Si, Al, Fe, Ca, Mg, Ti, Mn, Na, K, Sr, and Ba were found in abundance, reflecting their quality and production. Ca, Fe, and Mn are common elements whose concentration tends to vary for different samples. The application of kernel principal component (KPCA) with PCA and backpropagation neural networking (BP-NN) is used for the classification of ceramics. KPCA is a nonlinear form of standard PCA, where an integral operating kernel function computes the principal components in a high-dimensional feature space. It implicitly relates the input space to a feature space through nonlinear mapping [64, 65, 66].

With the recent advancements in laser spectroscopy techniques and chemometrics, the potential growth in the applications of these techniques in forensic science can not be ignored [67, 68]. LIBS with PCA is applicable in examining the ink pen spectra of questioned documents. LIBS was implemented to study the composition of black gel pens samples of different brands with minimal damage to the specimens. The samples were then successfully classified with PCA, proving the combination of these two methods is a way to rapid, in-situ characterization of forensic samples [69]. Soil serves as good evidence for forensic purposes as it has a large variety of minerals and trace elements

present in it. The chemical characterization of soil samples from similar and different origins could be beneficial for forensic purposes. Therefore, soil samples collected from five different sites were studied under LIBS and LA-ICP-MS techniques. In addition to that, a forensic spatial/sampling heterogeneity study was conducted to check the variability on spatial scales between sites, within sites, within sub-plots, and within samples. This avoids misclassification of samples that are similar-looking and aids in forensic casework. The elements selected for classification with the LA-ICP-MS technique are the isotopes of Al, Ba, Ca, Li, Mg, Sr, Ti, U, V, Zr, and those obtained with LIBS are Ba, Ca, Cr, Cu, Fe, Li, Mg, Mn, Pb, Sr, Ti, and V. Ratios between $\frac{SrII}{TiI}$, $\frac{Ba-II}{MgI}$, $\frac{CaI}{MgI}$, $\frac{FeI}{MgI}$ and $\frac{LiI}{MgI}$ are considered to perform the classification. PCA could successfully discriminate between the soil samples of two different sites and three standard reference materials. Also, the classification between the three study sites was successfully done with PCA [70]. Glass samples are major evidence in the case of forensic investigations. Therefore, extensive studies have been done to characterize the glass samples with LIBS. The work of E. M. Rodriguez-Celis and his group demonstrates the application of LIBS with refractive index (RI) determination to identify glass samples with similar RI. Here, the sample classification is done by recording the unique spectral fingerprints of LIBS with linear and rank correlation methods. The linear relationship between two intensity variables is estimated using the linear correlation method. In the case of the rank correlation method, these variables are replaced with their respective ranks. Apart from this, spectral masking, which allows the elimination of analytically useless parts of the spectra and retains selected peaks through the multiplicative process, is

employed. This approach makes LIBS a robust technique to analyze foren-sic glass samples [71]. Similarly, comparative studies have been conducted to analyze glass samples with different spectroscopic methods. The results show the superiority of LIBS and LA-ICP-MS techniques. The accuracy and precision of the latter method are better compared to LIBS. The advantage associated with LIBS is that the classification of glass samples with similar RI is possible just by comparing the emission spectra [23, 24]. The impor-tance of LIBS with a combination of chemometrics is recorded for classifying various biomaterials and chemical warfare simulants. Biological agent stim-ulants, which include various kinds of bacteria, biological interferents which consist of pollen grains, geological interferents, and chemical stimulants are elementally analyzed with LIBS and classified with PCA and SIMCA. The classification with PCA is performed for single-shot and averaged spectral data for all classes of samples. The classification results are better obtained for averaged spectral data and are verified with SIMCA as well. [72].

Plastics and Explosives

The use of plastic goods in our daily activities has become inevitable. The accumulation of plastic waste and disposal issues are major consequences arising out of it. Therefore, a necessity arises to discriminate between the various classes of plastics and perform qualitative and quantitative analy-sis. Henceforth, the application of LIBS is beneficial in this field as well. The identification of plastic samples such as acrylonitrile-butadiene-styrene (ABS), polycarbonate (PC), polystyrene (PS), styrene-butadiene (SB), high-density polyethylene (HDPE), polyethylene (PE), polytetrafluoroethylene

(PTFE), polyamide (PA), low-density polyethylene (LDPE), polyphenylene oxide (PPO), polyoxymethylene (POM), polyethylene terephthalate (PET), polymathy methacrylate (PMMA), high impact polystyrene (HIPS), polypropylene (PP), thermoplastic polyester (TPO), chlorotrifluoroethylene (CTFE) and polyvinyl chloride (PVC) with LIBS are reported in literature [73]. The study by V. K. Unnikrishnan, et al, explores the application of LIBS to identify four kinds of plastic samples, viz., PET, high-density PE, PP, and PS. The recycling of these samples is required for economic, environmental and biological safety. The emission spectra obtained for all samples mark the presence of CN molecular bands, C and H, which identify the presence of organic compounds. The classification between samples is done with PCA, which forms distinct clusters for all samples. To further aid the results obtained with PCA, Mahalanobis distance (M-distance) was calculated for all samples [74]. In recent decades, there has been an exponential growth in the generation of waste electronic and electrical equipment (WEEE or e-waste). Therefore, six different kinds of polymers, ABS, PS, PE, PC, PP, and PA, which are mainly found in e-waste, are examined with LIBS. The emission lines of C, H, N, O and the molecular band of C_2 were taken as the variables. Classification was performed using PCA, SIMCA, DSC, and KNN. The classification between ABS and PS was not clear with PCA as they possess similar properties. Therefore, the results were further refined with other chemometric techniques [75]. Similarly, e-waste generated from different polymer parts of mobile phones of different brands was studied with LIBS. Emission lines of different elements were observed for different kinds of polymers. Classification of polymers is successfully performed with PCA. As

polymers are made of organic elements, LIBS with chemometrics is a suitable approach to explore them [76].

The application of stand-off and remote LIBS for the detection of high-energy materials (EM) is a fast growing technique. With the improvement in laser wavelength, signal enhancement of LIBS, and most importantly, the capability of LIBS to detect organic elements, it has become suitable for analyzing explosive materials and classifying them with chemometric techniques like PCA, SIMCA, and PLS-DA. Femtosecond pulses are advantageous for the detection of explosives because short-duration energy is captured by the material and less attenuated by the environment. Therefore, rapid ionization with less thermal and mechanical damage makes it precise for laser ablation [77]. The application of standoff and remote femtosecond LIBS was reported for the detection of explosives like Nitroimidazoles and Nitropyrazoles, which are nitro-rich energetic molecules. Standoff LIBS were employed to examine five kinds of nitroimidazoles at different distances. Considering the important spectral features of C, CN, PCA has successfully classified the samples at all studied distances. Remote LIBS was used to examine nitroimidazoles and nitropyrazoles along with metal and alloy targets at a distance of 8.5 m away. C, H, N, O, and molecular bands of CN, C_2 are the main spectral features of HEM's. A successful classification of HEM's and target metals was achieved with PCA for remote LIBS analysis as well. This highlights the potential of LIBS and PCA to analyze and classify HEM at a distance location [78]. The study of pure explosives and residual explosives as an organic interferent is done with single-pulsed LIBS. Atomic lines of C, H, N, and O were observed along with the emission lines of Al, Fe, K, Mg, Ca,

and Na, which are due to impurities. In addition, molecular lines of CN and C_2 were also detected. The ratio between O/N, O/C, H/C, N/C, and O/H was taken for PCA classification. Classification of three explosive samples was successfully achieved using PCA. To improve the classification, differences in chemical reactions occurring in plasma were taken into account as a parameter for PCA [79]. The study has been further extended by the same authors to obtain a clear distinction between residual and organic interferents by taking into account various spectral parameters. The result suggests nonuniform variation in plasma temperature and electron density for types of samples is a factor to be considered to improve the classification of energetic samples with LIBS [80].

1.3.3 Importance of LIBS with PCA in the analysis of biological samples.

The first biomedical application of laser was found in 1968. The Ruby laser was used to fragment urinary calculi, but due to continuous heat generation, its clinical application was not found to be feasible. The invention of laser lithotripsy in the mid-1980s for the treatment of stones marked the era of the laser in the field of biomedicals. Over the years, the application of laser in this particular field has extended to the analysis of bones, teeth, hair, blood fluid, eyes, skin, cancer, etc. The development of laser technology in the field of medicinal science was further aided by the advent of LIBS. It opens wide opportunities for analytical inspection of biomedical samples due to the various versatile properties that are associated with the technique. The

biomedical application of LIBS is classified into the following two categories:

1. Mineralized tissues which involve the analysis of bones, teeth, hair, kidney/urinary/gallbladder stones.

2. Soft tissues which involve the analysis of organs, detection of pathogenic microorganism and malignant tissue [5].

Study of the biological sample and its classification was further enhanced by the introduction of the multivariate analysis technique. Marvelous progress has been made in LIBS-based classification of biological samples related to forensic purposes, cancer diagnosis, dental care, characterization of stones, age classification, etc [5],[13, 14, 81]. Here we discuss some major progress made in this particular field by the application of LIBS with multivariate analysis

Application of LIBS for the analysis of soft tissue.

There are two methods for detection of human soft tissue with LIBS, viz. pathological and physiological detection. The former method involves the detection and classification of malignant and normal tissue, and the latter method deals with the identification and classification of normal tissue [82]. The pathological application of LIBS is found in the discrimination between cancerous and normal human tissue from the breast, colon, larynx, and tongue. In-vitro analysis of trace elements for normal and malignant tissue extracted from these parts is compared. Higher concentrations of trace elements were recorded for malignant tissues compared to normal tissues.

Malignant breast tissues had the highest concentration of trace elements and the lowest concentration of trace elements were found in malignant colon tissues. Apart from the concentration of trace elements, the plasma temperature and electron density are found to differ for both kinds of tissue. Therefore, the concentration of elements along with plasma temperature can be utilized to discriminate between samples. The results of LIBS are further supported by ICP-OES and QP-MS [83]. The application of LIBS was reported for the identification of cervical cancer from normal tissue, which is the most widely occurring cancer in women. The LIBS spectra show the presence of Ca, Al, Na, K, and Mg in both normal and malignant tissue. A higher concentration of trace elements like Na, K, and Mg are found in infected tissues. The classification between two samples was performed with PCA, where clear classification could not be achieved. Therefore, support vector machine (SVM) and combination of PCA-SVM is done to improve the identification [84]. Similarly, a vitro study for the identification of malignant and non-neoplastic breast and colorectal tissue at different stages is explored with LIBS. Emission lines of Ca and Mg are recorded from the LIBS spectra for both tissues, but the concentration of these elements is higher for malignant tissue. The intensities of these elements are compared at different stages of growth for both malignant and non-neoplastic samples and are found to vary at each stage. This shows the capability of LIBS to perform vitro analysis of malignant cells and is a promising technique for clinical application for detection of cancer in the near future [85]. The feasibility of LIBS to examine cutaneous malignant melanomas and surrounding dermis tissue is being studied. Here, melanoma tissues were implanted on mice and

samples were divided into two classes: in the form of pellets and surgically extracted. C, Mg, Ca, Na, H, Na, K, O, and Cl were detected with Ca and Mg showing major variance in malignant and normal tissue. PCA was employed to classify between melanoma and dermis cells and better classification was obtained for samples in pellet form. The classification was further testified by LDA as well. Therefore, these studies highlight the advantages of using LIBS over histological methods [86]. LIBS has emerged as a good candidate for real-time investigation of hepatic cirrhosis. Different stages of hepatic fibrosis in rat liver tissue are studied with LIBS. An increase in the intensity of Ca is observed as the stages of fibrosis progress. The application of PCA is found here to classify among different phases of the disease [87]. The physiological application of LIBS is reported for the identification of normal tissue from the brain, lung, spleen, liver, kidney, and skeletal muscle extracted from a chicken. The emission lines of Ca, Al, Fe, Cu, Na, Zn, Cr, Mg, K, P, C, Li, Ni, Mo, Sn, and Sc are observed in the LIBS spectra of samples, but Ca shows maximum intensity and variance for different organs. PCA, ANN, PLS-DA, HCA, and DFA are the approaches adapted to perform the classification. PCA is used as a preliminary technique for the reduction of collinearities in data and data reduction. The classification was further refined with PLS-DA and ANN [88].

Application of LIBS for the analysis of hard tissue.

The contribution of LIBS can not be ignored when it comes to the analysis of several calculi and stones occurring in different organs of the human body. In the year 2005, for the first time, LIBS was used to analyse sev-

eral types of urinary calculi [81]. Here, major and trace elements present in the samples were identified from the LIBS spectra. After this, a series of works have been published in this particular field that have proved LIBS as a promising technique for identification and classification of various kinds of human stones. A quantitative analysis of gallstones was performed with calibiration free LIBS (CF-LIBS). The results obtained from LIBS are compared with those obtained from the ICP-AES technique. The gallstones are classified into pigmented, cholesterol and mixed types based on their cholesterol, bilirubin content and colour. Emission lines of Ca, Mg, Mn, Cu, Fe, Na, K, Sr, Zn, C, H, N, O, and P are recorded for the pigmented type, where as Zn and Sr are absent in the cholesterol type. The presence of Mg and Fe was not recorded with the ICP technique, but LIBS showed large emission lines of these elements. Detection of C, H, N, and O marks the presence of organic compounds which were not detectable with ICP methods. Ca is the most abundant element recorded. Therefore, the ratio of all other elements with respect to Ca is evaluated and compared to calssify the samples. Study concludes that the origin of all kinds of gallstones are the same but their properties are altered by their growing process[89]. This study was further extended to study the concentric rings inside the gallstones with LIBS in air and argon medium. Cu, Fe, Na, and K were found in variable amounts in the light and dark bands, whereas C was abundantly found in both the bands as it is the major constituent of cholestoral and bilirubin. Here, the evolution of swan bands of C_2 and voilet bands of CN are studied to estimate their presence in gallstone. Also, the evaluation of these bands allows easy calssification of samples. The results track the origin of C_2 are from sput-

tering of cholesterol, bilirubin, and hydrocarbons already present in stones. The origin of CN is mainly due to decomposition of organic compounds or due to recombination of excited carbon atoms in hot plasma plume and nitrogen in air. This has been resolved by performing the experiment in an argon atmosphere and confirming its presence is due to organic decomposittions [90]. The study was further extended to classify the cholesterol and pigmented gallstones with PCA based on emission lines of C_2, C, and Mg as these are the signature elements found in both kinds of stones. A clear classification between two kinds of samples are obtained with PCA which is shown in fig.1.1 [91]. This shows the robustness of LIBS for identification of gallstones and its importance in the clinical application [91].

Kidney stone is again one of the major human ailments which needs to be examined closely. It occurs in various locations and is named accordingly, such as renal/kidney stones, ureteral stones, bladder stones, and urethral stones. Due to the ability to perform rapid elemental analysis and to detect a wide range of elements, LIBS is found applicable for studying varieties of kidney stones. Five different kinds of stones extracted surgically are studied cross-sectionally and by taking samples from the surface, shell and center. The LIBS spectra obtained for pulse energy ranging from 10-40 mJ per pulse show the emission lines of Ca, Mg, Cu, Fe, Zn, Sr, Na, K, P, S, Cl, and lighter elements like C, H, N, and O. The presence of Ca and P indicates the stones are calcium phosphate, whereas the elements such as S and Ca, Mg and Ca suggest they are gypsum and dolomite. The presence of Na, K, and Cl indicates the formation of halides during the initial precipitation phase. The results obtained with LIBS were verified with those obtained from
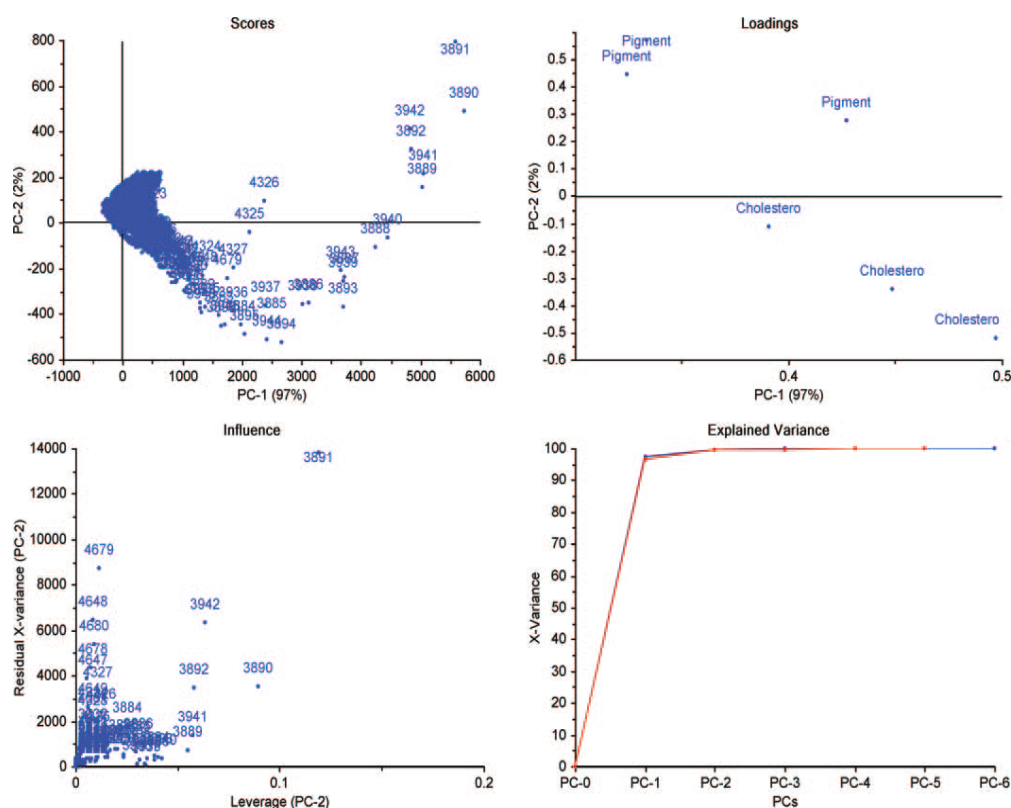
Figure 1.1: The figure shows the application of PCA used to classify between cholesterol and pigment gall stone.[91]

ICP-MS and as Ca was the most abundantly occurring element, it concludes that the stones were calcium oxalate in nature. The concentration of trace elements was estimated through calibration curves and the intensity ratio of elements with Ca was done to find the spatial distribution of elements inside the samples. Therefore, LIBS allows one to estimate the origin of kidney stones through quantitative estimation of elements [92]. The application of single pulsed LIBS is found to estimate the carcinogenic elements in kidney stones that result in harmful kidney disorders. The toxic elements detected

were Cr, Pb, Cd, along with Ca, P, Zn, Ni, and V. The concentration of these elements is measured with a calibration curve and compared with the ICP technique. Apart from this, the dependence of intensity on laser energy, time delay, and other plasma parameters are listed in this work [93]. Urinary stones were first studied with LIPS and were divided into seven categories according to colour and composition. With the advancement of LIBS, it was restudied and divided into four categories, viz., oxalate, phosphate, uric acid, and cystine stone. About 70% f the urinary stones are composed of calcium oxalate. Uric acid and cystine are less frequently occurring urinary calculi and do not contain Ca [94, 95]. To classify between organic and inorganic calculi, a micro-LIBS system consisting of a higher-energy laser and an Echelle spectrograph with an ICCD camera is designed [96].

Human nails are hard tissue that consists of keratine and stable proteins. Therefore, it bears trace elements for a long period, which upon elemental analysis can be useful for detection of various mechanisms that are going on inside the human body [81]. A study focuses on the diagnosis of nails infected with onychomycosis, a fungal disease, through elemental analysis with LIBS. The normal region and pathological region with yellow and brown colours are examined under LIBS, which shows the emission lines of Ca, Na, and K. The intensity of these elements is found to vary across the various normal and affected regions of samples. The intensity ratio of elements with K is evaluated as it has weak emission lines and less self-absorption effect. The transient temperature is studied for all the inspected regions with violet bands of CN radical, which allows one to estimate the error in the intensity of emission lines [97]. The utility of LIBS is tested for discrimination of human

fingernails based on sex and age. The elements detected with LIBS were Al, C, Ca, Fe, H, K, Mg, N, Na, O, Si, Sr, Ti, as well as the CN molecule. A higher concentration of Al, CN, Fe, H, K, Mg, Na, O, and Si was observed in men's fingernails. Whereas, a higher concentration of Ca and Ti was obtained for women's samples. The correlation between the concentration of elements is achieved with the Pearson correlation technique. O, N, H, CN, Fe, and Ca are elements useful for discrimination of sex and age indication with DFA. Though a clear classification of age could not be obtained, identification of a particular age group was possible with these methods [98]. Discrimination function analysis (DFA) is utilized to discriminate the sex and five age groups with the fingernail samples which is shown in fig.1.2 [98].

Human bone is a calcified tissue of organic and inorganic origin which mainly consists of hydroxyapatite, water, carbonates, phosphates, collagen and proteins. Calcified tissue has a longer decay time and can preserve resources that occur due to environmental, nutritional, pathological changes etc. Therefore, its study is important for archeological, anthropological, forensic, and medical purposes [81, 5]. With LIBS, the study and classification of bones are extensively performed, few of which are discussed here. The study of ancient cattle bovine bones that are 4600 years old and recent bovines are studied with LIBS that is enhanced by biosythesized silver nanoparticles (NELIBS). The sample classification is based on the fodder that was consumed in ancient times and contemporary times. The spectra of ancient bones showed sharp emission lines of Si, Fe, Ca, Ti, Mg, Na, but the recent samples had the emission lines of C, CN along with Ca, Fe, Mg, Na. The hardness of both samples are compared by taking the ratio of atomic
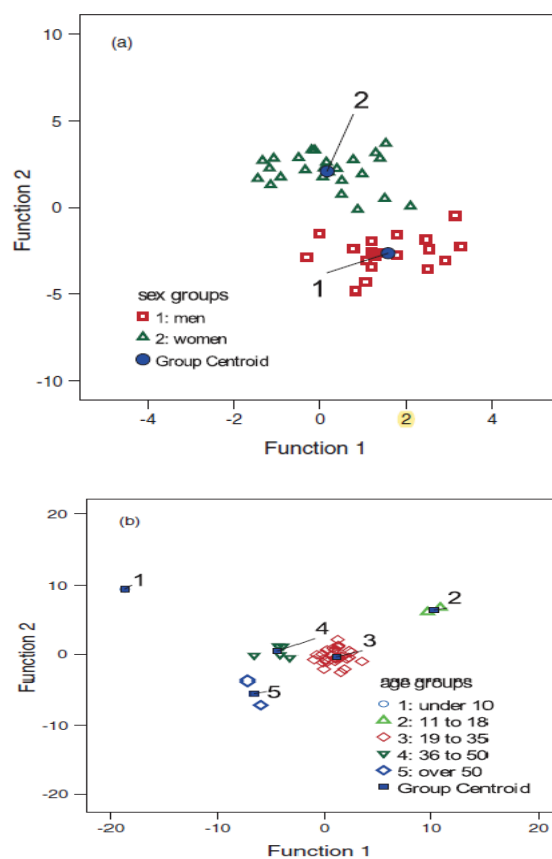
Figure 1.2: The figure shows the application of DFA used to classify human nails on the basis of sex and age [98].

to ionic lines of Ca and Mg and the LIBS spectra of both are classified with PCA shown in fig.1.3 [99].

Apart from bones, different kinds of fodder used to feed cattle were studied as well, to trace the presence of elements that might have been incorporated into bones. Clover, barley, and artificial feed are the three samples studied under NELIBS where elements like Si, Ti, Fe, Ca, Mg, and Na are detected. The PCA plot is observed for each of the fodder with bone samples to examine the correlation between dietary habits and bone samples. Here,
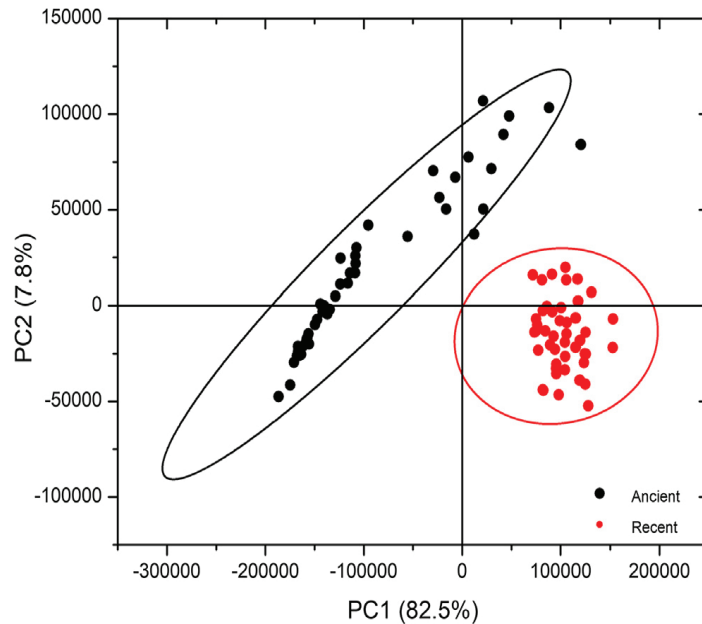
Figure 1.3: The figure shows application of PCA used to classify the ancient and recent bovine bone samples of animals [99].

PCA could provide a clear classification between ancient and recent bovine bones, but it failed to establish a correlation or influence of the primitive and recent feeding habits on the bone samples [99]. The Temporomandibular joint (TMJ) leads to restricted movement and pain in the cartilaginous discus articularis, the cartilaginous surface of the condyle, or bone. Therefore, removal of TMJ-affected tissue with a laser may damage the non-affected tissues as well. A study aims at the identification of cartilage and cortical bone tissue with LIBS to set a basis for laser surgery and widen its clinical application. Tissues were extracted from pigs in an ex-vivo time frame to avoid time alteration. The emission lines of Ca, Na, K, and CN were recorded and the intensity ratio between Ca, Na, and K was evaluated and

compared with both the samples to differentiate them. As sharp emission lines were obtained for the cortical bone, ratio values were higher for it as compared to cartilage tissue. PCA is applied here to classify between the two samples for the entire LIBS spectra. Firstly, PCA is used to classify the tissues for all five samples and is again projected for a single sample. Better results are obtained when PCA is applied to individual samples, as shown in fig.1.4 [100]. The dimension is highly reduced by PCA and the first ten PCs are used as input data for LDA to further refine the results. This shows the efficiency of LIBS with multivariate analysis as a clinical tool for real-time investigation of tissues [100]. The application of laser in dentistry
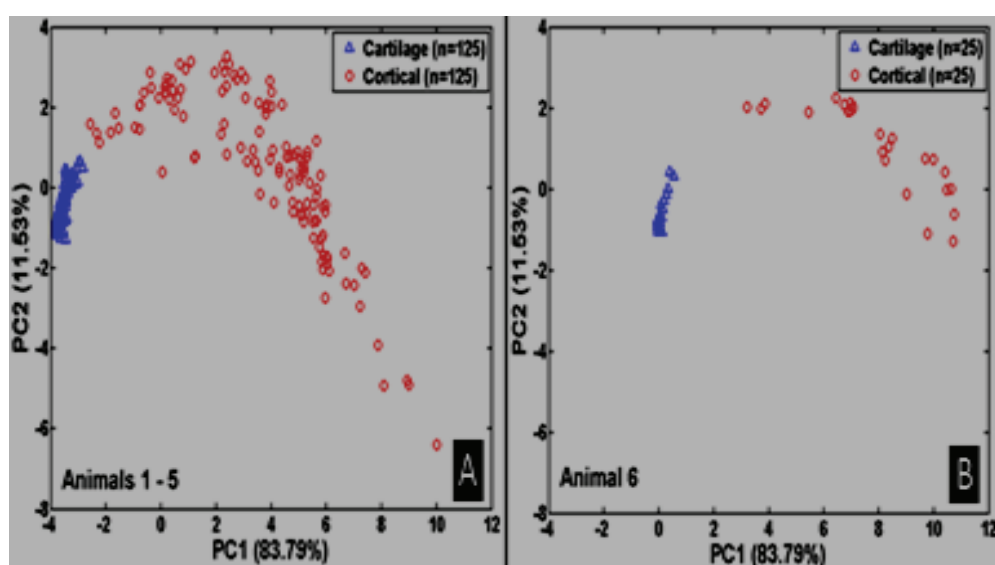
Figure 1.4: The figure shows application of PCA to classify the cartilagious and cortical bone tissue [100].

cannot be ignored, laser is found applicable in curing many dental amalgams. The properties of LIBS to perform rapid elemental analysis for solid samples

and the identification of both organic and inorganic elements has made it a versatile technique for teeth analysis. Again, teeth and bones are stable calcified tissue that can bear biological fingerprints and contaminations that are retained for ages. Therefore, it serves a great purpose in understanding the changes that have occurred in animal and human physiology with the advancement of civilization. Its importance cannot be ignored in the field of forensics as teeth can preserve DNA for human remains. By estimating the hardness of teeth age estimation could be performed. The study of human teeth for medical, archeological, forensic purposes has increased to the manifold with LIBS as it can retain biological information and is easily accessible [5, 13, 81, 101, 102]. Here we highlight recent progress made in the field of dentistry with the application of LIBS. A human tooth is one of the hardest calcified tissue, crystalline in nature and is composed of a mineralized compound hydroxyapatite [$Ca_{10}(PO_4)_6(OH)_2$] [5, 103, 104]. Therefore, Ca and P are major elements found in a human tooth along with the presence of trace elements like Cl, F, Na, K, Sr, Mg, Mn, Cu, Zn, Pb which are incorporated due to various environmental conditions during teeth formation and dental conditions [103, 105]. The human tooth is divided into three regions viz., enamel and dentin which forms the crown region, and cementum forms the root. Enamel is composed of 96% of mineralized inorganic material and 4% organic material and is the hardest and mineralized section. Dentin consist the pulp and is made of 70% mineralized inorganic material, 20% organic material and 10% water and cementum contains 65% mineralized inorganic material 23% organic mineral and 12% water [106, 107].

The first study on human teeth samples with LIBS was reported by Samek,

et al, where trace elements in human teeth due to a whitening agent in toothpaste and dental fillings were examined. Quantitative detection of both major elements along with detection of elements like Ag, Al, Ca, Cr, Hg, K, Mg, Mn, Na, Ni, P, Sn, Ti, and Zn were reported. The presence of Al and Ti are due to whitening agents found in different kinds of toothpaste. These are beneficial trace elements as they prevent teeth from corrosion. The presence of Hg, Sn, Zn, Ag is due to fillings of amalgams that contain a mixture of some metals. They have investigated the study for infant, child, and adult teeth samples [108]. The same author has extended the work to investigate the clinical application of LIBS to analyze teeth and dental materials. Here they have elaborately discussed the effect of whitening agents, dental fillings, and orthodontic braces on the accumulation of trace elements in teeth. The spatial distribution of elements across the teeth section and detection of elements with depth profiling technique were studied [109]. This provides an initiating point for the investigation of teeth with LIBS and brings out the robustness of the technique for clinical application. The next important study in this field is the identification of caries-infected teeth samples. Dental caries or tooth decay, is one of the leading problems associated with dental health. Caries infection occurs when the acid corrodes the surface of the enamel by replacing the matrix elements like Ca and P with trace elements like Mg, Sr, etc. Therefore, there arises the need to examine the infection at the initial stages to prevent pain and loss of a tooth. A study of caries with LIBS shows that there is an increase in the concentration of trace elements like Mg, C, Cu, Zn, Sr, Na, and K in the affected region. The intensity ratio of these elements with Ca (C/Ca, Mg/Ca, Na/Ca, Sr/Ca, and K/Ca) shows the higher concen-

tration in the infected region compared to the healthy once [105]. Therefore, the strength of enamel decreases with the infection of caries, making the teeth porous and brittle. The LIBS spectra of the healthy and infected region within the range of 200-850 are shown in fig.1.5 [105]. The importance
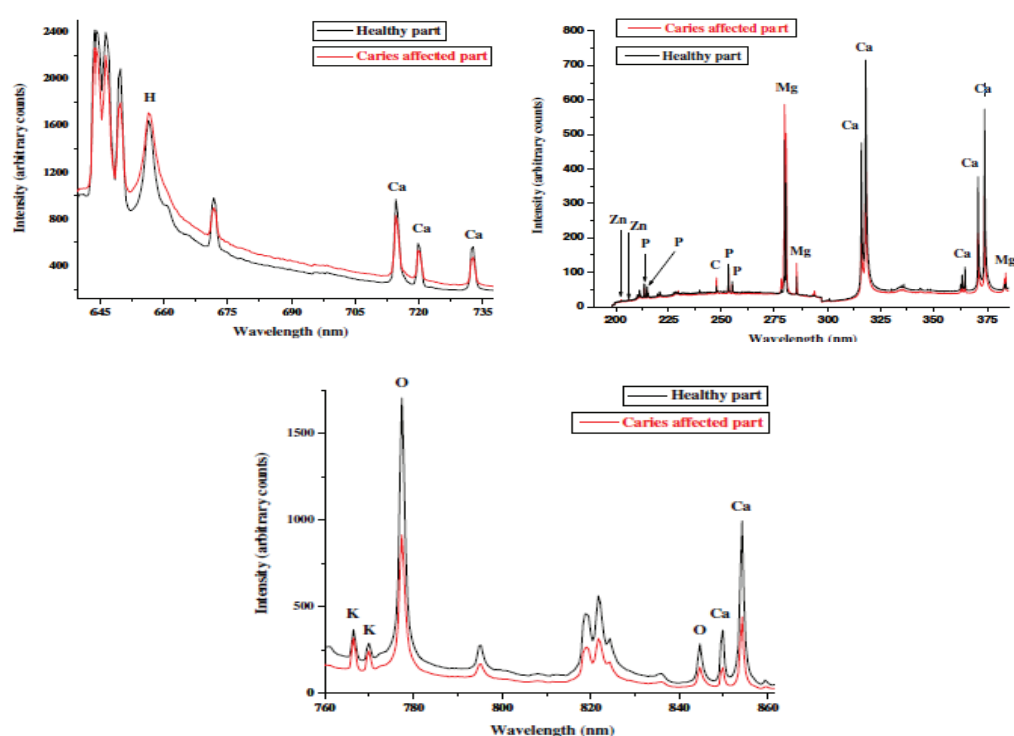
Figure 1.5: The figure shows LIBS spectra for the healthy and caries infected teeth samples. [105].

of LIBS as a real-time in-vivo and in-vitro investigation of caries is reported by Samek, et al., an algorithm was designed for Discriminant Analysis which serves two purposes: detection of material purity/quality determination, and

material identification/screening. After the identification of samples by DA, Mahalanobis Distance (M.Dist) is the technique adopted for matching the LIBS spectra of tooth samples and mapping of caries teeth. The intensity ratio values of Ca to Mg were evaluated for each healthy and affected sample batch. Classification between two samples was obtained for both in-vivo and in-vitro experiments. This study sets a principle for in-vivo identification of caries, bringing out the ability of LIBS in combination with algorithms, to be a promising technique for caries treatment [110]. The application of PLS-DA is reported for the classification of healthy and caries-infected teeth for the enamel and dentin parts of the sample. Here, classification is based on the emission lines of P, Ca, Mg, Zn, K, Sr, C, Na, H, and O for both parts of the sample. Clear classification of healthy and caries for both sections has been achieved. Also, classification of unknown samples from both sections has been achieved [111]. Apart from this, many works are found in literature where the robustness of LIBS for caries identification and the morphological changes that occur in it due to infection are well studied. Also, LIBS provides the platform to understand the original tooth matrix and the spatial arrangement of elements in it [103, 104].

To discuss the forensic and anthropological application of human tooth samples with LIBS, it is noted that elements like Ca, Mg, and Sr are important for forensic investigation. These elements are readily found in human teeth samples, therefore identification becomes easier [81]. Sea-water drowning has been investigated by LIBS by examining dental samples. Spectral features of dentin and enamel were recorded, which showed the higher concentration of Sr was observed in the dentin part of the drowned body [112]. The

other application is in the classification of human bones and teeth fragments to identify remains. As discussed earlier, teeth bones can retain biological imprints, therefore LIBS can provide less costly and rapid identification of human remains. This classification has been achieved by the application of neural networking (NN) based on the emission lines of Ca, Sr, and Mg. Satisfactory results are obtained and the method is less costly and more rapid as DNA analysis is not required [113]. The teeth samples from different civilizations and different historic periods, based on their habitats and adaptations, have been studied with LIBS. A significant difference in the concentration of Ca, Pb, Al, Sr, Mg has been recorded [114]. Also, the difference in the concentration and different types of trace elements are detected in the samples of people involved with smoking, drug addiction and dietary deficiencies [115].

The hardness of a calcified tissue can be measured by estimating the ratio of ionic to neutral lines of Ca and Mg. In a study, the hardness obtained from the ratio of spectral lines was compared with the standard Vickers hardness number (VHN) for different calcified tissues. It confirmed that the ratio of ionic to neural lines of Ca and Mg gave correct values. Furthermore, it was more accurate for Mg as it is less abundant and the effect of self-absorption is neutralized [116, 117]. Utilizing this factor, micro spatial analyses of prehistoric bear dentin were studied with LIBS, LA, and ICP-MS. Sr, Ba, Fe, Ca, P, Na, and Mg are elements observed. The ratio between Sr/Ca and Sr/Ba helped to estimate seasonal fluctuations that proved the migration of this bear between his hibernation location and the place where fossils were located. The ratio of ionic to neutral lines of Ca and Mg was used to esti-

mate the hardness of the sample [118]. A study was conducted to analyze the hardness of enamel, dentin, and cementum parts of human teeth samples by estimating the ratio of ionic to neutral lines of Ca and Mg was taken from the LIBS spectra. Here, the hardness estimated for different age groups was found to vary with age for the enamel and cementum sections. The study concluded with the application of PCA to classify the different sections of human teeth samples, and it showed that enamel is the hardest section of human teeth samples [12]. From the above review of literature, we conclude that LIBS is a rapidly emerging technique in the field of laser science. Satisfactory applications of LIBS are found in almost every scientific field. The biological application of LIBS is a rapidly growing scientific advent, especially in the investigation of calcified tissues. Its importance is not limited to biomedical only, but is important from a historical and forensic point of view as well. Therefore, the motive of our work is to estimate human teeth samples of varying ages with LIBS and to perform age classification by combining various multivariate techniques.

Chapter 2

Materials and Methods

2.1 Materials

The clinically removed teeth samples from the age group of 5-60 years were collected from Kalimpong Sub-Divisional Hospital. The samples were divided into six different age groups. A total of 12 samples has been analyzed. The samples were dissected vertically into two halves and examined, with the help of a dental surgeon, to study the enamel and cementum part separately. The samples were then cleaned with distilled water to remove all the surface contaminations and then dried at room temperature. The sample image is shown in fig.2.1. The drawback faced during the samples collection is the absence of a proper medical history of the patients. Since these are clinically extracted samples a hint of caries infection is present in all the samples. Though, care has been taken during the experiment so that the healthy section is exposed to the laser. However, the presence of contamination cannot be ruled out.

47
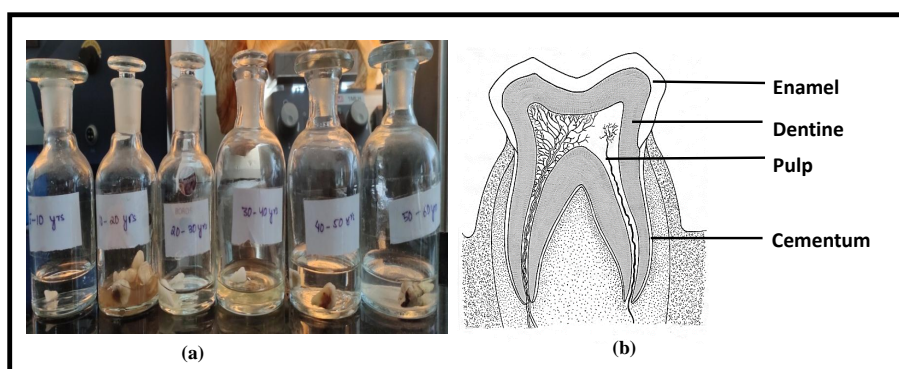
Figure 2.1: a) Clinically removed teeth samples between the age group of 5-60 years collected for the study. b) The vertical crossection of a tooth showing different parts of it.

2.2 Methodology

2.2.1 Experimental setup

LIBS is adapted to experimentally examine the teeth samples due to its efficiency to perform the rapid elemental analysis of biological samples specially for the hard calcified tissue. The schematic diagram of the experimental setup is shown in fig.2.2. For each age group, two different target points were set and the LIBS spectra for both the enamel and cementum sections of the samples are obtained for the study. A beam of pulsed Q-switched Nd:YAG laser(Litron Laser, LPY 707G-10) at wavelength 1064 nm is employed for the experiment. The pulse is focused on the enamel and cementum part, using a quartz lens of focal length 15 cm. The emission from plasma is collected at

45 degree angle to the incident laser beam, with the help of radiation collection optics and spectrometer (Ocean Optics USB 2000+ working in windows 2007 professional; mode) equipped with a charge coupled device (CCD).
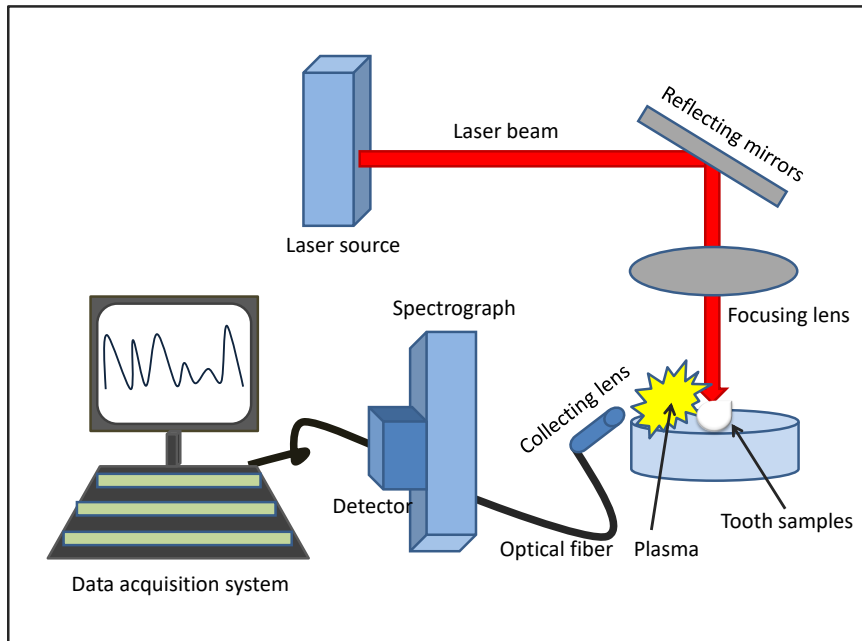
Figure 2.2: Figure shows schematic diagram of the experimental setup.

2.2.2 1D Classification

The hardness of samples, which is proportional to the ratio of ionic to neutral lines of Ca and Mg, is first analyzed with 1D classification method with a histogram plot. Following three ratios were evaluated: $\frac{CaII(422.7nm)}{CaI(442.67nm)}$, $\frac{CaII(500.148nm)}{CaI(442.67nm)}$, $\frac{MgII(525.44nm)}{MgI(517.169nm)}$. A histogram shows a statistical distribution of data over a range of variables. This method tests the variation of these three ratios concerning age groups for both the studied teeth sections. It provides us with information about the ratio having more variations with ascending

age and could contribute to the classification. Also, variation of these ratios in the enamel and cementum part for every age group is tested with a histogram. This allows one to establish a comparative figure amongst the two sections of the same sample

2.2.3   2D Classification

To bring out the classification image hidden in these ratio values 2D analysis is performed. For this the values of ratios $\frac{CaII(500.148nm)}{CaI(442.67nm)}$, $\frac{MgII(525.44nm)}{MgI(517.169nm)}$ were taken in the form of a matrix, which forms the two variables X and Y of analysis. The method is based on the multivariate normal distribution function given by the following equation

$$f(x) = \frac{1}{(2\pi)^{r/2}|\sigma|^{1/2}} \exp[-\frac{(X-\mu)'\sigma^{-1}(X-\mu)}{2}] \qquad (2.1)$$

Where, r are the number of dimensions, σ is the covariance matrix, and X, μ are the matrix of variables and its mean respectively [120]. The expression $(X-\mu)'\sigma^{-1}(X-\mu)$ is the square of distance between the experimental point X and the mean μ. A multivariate normal distribution is a constant on the surface where the square of distance is a constant. Such paths are called the contours and contours of constant density for r dimensional normal distribution forms an ellipsoids defined by the paths of X shown in fig.2.3.

$$(X-\mu)'\sigma^{-1}(X-\mu) = (a)^2 \qquad (2.2)$$

These ellipsoids are centered at μ whose axes are defined by $\pm a\sqrt{\lambda_i}e_i$, where λ_i and e_i are the eigenvalues and eigenvectors of the covariance matrix. For this study the above distribution function is reduced to the bivariate normal distribution function, with following expression

$$f(x,y) = \frac{1}{2\pi\sqrt{\sigma_{xx}\sigma_{yy}}(1-\rho_{xy}^2)}\exp[\frac{-Z}{2(1-\rho_{xy}^2)}] \qquad (2.3)$$

Where,

$$Z = (\frac{x-\mu_x}{\sqrt{\sigma_{xx}}})^2 + (\frac{y-\mu_y}{\sqrt{\sigma_{yy}}})^2 - 2\rho_{xy}\frac{x-\mu_x}{\sqrt{\sigma_{xx}}}\frac{y-\mu_y}{\sqrt{\sigma_{yy}}} \qquad (2.4)$$

Here μ_x and μ_y are the mean values and σ_{xx} and σ_{yy} are varaince of vari-

Figure 2.3: The image shows countour formation in the with 2D distribution function.

able X and Y respectively. ρ_{xy} is the correlation coefficient between X and

Y [119, 120]. If, λ_x ,λ_y and e_x , e_y are the eigenvalue and eigenvectors of the covaraince matrix. For a positive covariance σxy, λ_x will be the largest eigenvalue and the associated eigenvector e_x lies along 45° through the mean points with $\pm a\sqrt{\lambda_x}e_x$ will form the major axis and $\pm a\sqrt{\lambda_y}e_y$ will be the minor axis of the ellipse and vice versa for negative covaraince. The diagonal elements of the covariance matix determines the spread of distribution region.For equal diagonal elements the distribution will be circular otherwise it is elliptical as shown in fig.2.3. The other important aspect of this method is the euclidian distance between the mean points of distributed regions. The countour lying at the center from which all other distribution region are at equidistant is taken as a focus point. The distance is calculated with respect to the mean points of this selected region to all the mean point of the rest region. A larger euclidian distance implies samples are more separated from each other and classification between them is more prominent.

2.2.4   PCA

The next method adapted to widen the picture of classification is the Principal Component Analysis (PCA). In recent years PCA has evolved to be an efficient tool in handling a large amount of data. Due to this efficiency of PCA, recently it has a wide application in the LIBS community. It has two major objectives:

1. Efficient data reduction.

2. Pattern formation of the reduced data without losing the originality of main data with a suitable [7, 8, 9, 10, 121].

PCA can be looked upon as the extension of a multivariate distribution function from two to "n" numbers of variables. Here the data for "r" measurements on "n" variables are taken in a form of a matrix. In the case of LIBS, "r" measurements are the wavelengths, and "n" variables are the intensity of emission spectra. The wavelengths form the rows, and the intensity of the spectra forms columns of the sample matrix. The beauty of PCA is that these "r" measurements on "n" variables are reduced to "r" measurements on "p" Principal Components (PCs). This is of importance as the entire variables are reduced to space formed by the PCs, without losing the identity of original data. Also, it enables the formation of patterns that are actually present in the original data and provides a suitable interpretation. Now we briefly look into the theory behind PCA. The aim here is to form a suitable basis to re-express the dataset as a linear combination of its basis vectors, assuming that there is a continuity in the set. Consider,a random vector $\boldsymbol{X} = [X_1, X_2, ...X_n]$ representing a certain variable, with a mean vector $\boldsymbol{\mu}$ and covaraince $\boldsymbol{\sigma}$ where $\lambda_1 \geq \lambda_2 \geq ....\lambda_n \geq 0$ are eigenvalues [120]. Let the linear combinations of the above set of variables be represented by the following equations:

$$Y_1 = a_{i1}X = a_{11}X_1 + a_{12}X_2 + ... + a_{1n}X_n$$

$$Y_2 = a_{i2}X = a_{21}X_1 + a_{22}X_2 + ... + a_{2n}X_n \qquad (2.5)$$

$$Y_n = a_{in}X = a_{n1}X_1 + a_{n2}X_2 + ... + a_{nn}X_n$$

Here $\boldsymbol{Y}$ is another vector related to $\boldsymbol{X}$ through the linear transformation $\boldsymbol{a}$, which re-represents the data set. Rows of $\boldsymbol{a}$ are the set of new basis vectors

for expressing the columns of $\boldsymbol{X}$. Each jth coefficient of Y_i is a projection on the jth row of $\boldsymbol{a}$ and are called the scores of PCA.

Therefore,

$$Y = aX \tag{2.6}$$

These linear combinations are actually the PCs of $[X_1, X_2, ...X_n]$ random variables. It sets a new coordinate system obtained by rotating the original set of coordinate axes through the rotation vector, $\boldsymbol{a}$. The new axes falls in the direction covering maximum variables and provides a clear description of the covariance structure. Let the variance and covriance in Y be given by the following relations:

$$Var(Y_i) = a_i' \sum a_i \tag{2.7}$$

$$Covar(Y_i, Y_j) = a_i' \sum a_j \tag{2.8}$$

Where $i, j = 1, 2, ...n$. The PCs are uncorrelated linear combinations of $Y_1, Y_2, ..., Y_n$, whose variance given by eq. 2.7 and these variance are equal to the eigenvalues of covaraince matrix $\boldsymbol{\sigma}$. Also, following relation holds:

$$\sum_{i=1}^{n} Var(X_i) = \sum_{i=1}^{n} Var(Y_i) \tag{2.9}$$

Therefore,

1st PC = linear combination of $a_1'X$ that maximizes the $Var(a_1'X)$ subject to the condition that $a_1'a_1 = 1$.

2nd PC = linear combination of $a_2'X$ that maximizes the $Var(a_2'X)$ subject to the condition that $a_2'a_2 = 1$ and $Covar(a_1'X, a_2'X) = 0$.

Similarly, i^{th} PC = linear combination of $a_i'X$ that maximizes the $Var(a_i'X)$

subject to the condition that $a_i' a_i = 1$ and $Covar(a_i' X, a_j' X) = 0$ for $j < i$.

Total population of variance= $\sigma_{11} + \sigma_{22} + ... + \sigma_{nn} = \lambda_1 + \lambda_2 + ... + \lambda_n$.

Population of variance for i^{th} PC= $\dfrac{\lambda_i}{\lambda_1 + \lambda_2 + ... + \lambda_n}$

If the first few PCs comprises most of the total population variance then these component can repalce the original n variables and reduce it into the sapce formed by PCs. As said earlier that the variance in $\boldsymbol{Y}$ is equal to eigenvalues of the covariance matrix of sample. Therefore, the PCs can be re-evaluated as following:

Let $\boldsymbol{\sigma} = \sigma_{ij}$ be the $n \times n$ sample covariance matrix

Let $(\lambda_1, \hat{e}_1)$, $(\lambda_2, \hat{e}_2)$,............, $(\lambda_n, \hat{e}_n)$ be the pairs of eigenvalues and eigenvectors associated with the matrix.

Therefore,

$$i^{th} PC = \hat{y}_i = \hat{e}_i' X = \hat{e_{i1}} X_1 + \hat{e_{i2}} X_2 + ... + \hat{e_{in}} X_n \qquad (2.10)$$

Provided, $\hat{\lambda}_1 \geq \hat{\lambda}_2 \geq .... \geq \hat{\lambda}_n \geq 0$ and

Sample variance $(\hat{y}_j) = \hat{\lambda}_j$, where $j = 1, 2, ..., n$

Sample Covariance $(\hat{y}_i, \hat{y}_j) = 0$, i$\neq$ j

$$\rho_{y_i, x_n} = \dfrac{\hat{e_{in}} \sqrt{\lambda_i}}{\sqrt{\sigma_{nn}}} \qquad (2.11)$$

The above is correlation coefficient between the Y_i components and X_n variables. Its values reflect the noise and redundancy in measurements. Therefore in summary

1. In PCA the basis vector taken for the transformation of original dataset

is assumed to be orthonormal i.e., $\boldsymbol{a_i}.\boldsymbol{a_j} = \delta_i j$.

2. The generalized rotation vector $\boldsymbol{a}$, selects a normalized direction in a "r"-dimensional space created by "r"- measurements along which the variance in $\boldsymbol{X}$ is maximum. Also it places PCs along the maximally variant axis.

3. Due to the orthonormality conditions, the search for rest of PCs are limited only in the directions pependicular to initially selected PCs directions.

4. Covariance matrix of the sample is of importance as it measures the degree of linearity between variables. The diagonal terms, which represent variance among the sample, large values of it indicate a good variance present in the sample, and small values imply noise. The off-diagonal, which are the covariance among samples, the large and fewer values of it implies high and low redundancy respectively. To reduce the redundancy and maximize the signal it is important to diagonalize the covariance matrix.

Now we look into the function that guides the formation of distributed regions, which helps to classify the samples. As said earlier that PCA is multivariate analysis. Therefore, the multivariate normal distribution function with few modifications guides the formation of contour. In the case of bivariate analysis, the samples were distributed in 2D space but in PCA the samples are distributed in the space created by "r" measurements. Consider $\boldsymbol{X}$ represent the sample matrix and is normally distributed in the region defined by $\boldsymbol{N_p}(\boldsymbol{\mu}, \boldsymbol{\sigma})$, where $\boldsymbol{\mu}$ and $\boldsymbol{\sigma}$ are the mean and covariance matrix of

$\boldsymbol{X}$. For the "r" dimension the distribution function is given by eq. 2.1 and for a constant density of $\boldsymbol{X}$, the distribution function is writen as:

$$(X - \mu)' \sigma^{-1} (X - \mu) = (a)^2 \tag{2.12}$$

This represents an ellipsoids which are $\boldsymbol{\mu}$ centered. If $(\lambda_i, \boldsymbol{e_i})$ be the set of eigenvalues and eigenvectors of $\boldsymbol{\sigma}$ then $\pm a \sqrt{\lambda_i} e_i$ defines the axes of ellipsiods. Therfore the length of the ellipsiods are proportional to $\sqrt{\lambda_i}$.

Now for convinience set $\boldsymbol{\mu} = 0$. eq. 2.12 reduces to

$$a^2 = X' \sigma^{-1} X = \frac{1}{\lambda_1} (e_1' x_1)^2 + \frac{1}{\lambda_2} (e_2' x_2)^2 + \dots\dots + \frac{1}{\lambda_n} (e_n' x_n)^2 \tag{2.13}$$

In the above equation the factor $(e_i' x_n)$ are the principal components of $\boldsymbol{X}$. Therefore the above equation can be rewritten as:

$$a^2 = \frac{1}{\lambda_1} (PC_1)^2 + \frac{1}{\lambda_2} (PC_2)^2 + \dots\dots + \frac{1}{\lambda_n} (PC_n)^2 \tag{2.14}$$

Therefore an ellipsiod is formed with $PC_1, PC_2, \dots, PC_n$ as the coordinate axes, in the direction of $e_1, e_2, \dots, e_n$. The largest eigenvalues (say λ_1) forms the major axis of the and lies in the direction of e_1. The rest of the eigenvalues forms the minor axis and falls in the direction defined by $e_2, \dots, e_n$. In general when $\mu \neq 0$, then for $\lambda_1 > \lambda_2$ the contour formed is elliptical and are μ centered as shown in fig.2.4. For $\lambda_1 = \lambda_2$, the contour is circular with the axes lying perpendicular to each other and the sample variation are homogeneous in all direction, shown in fig.2.5.
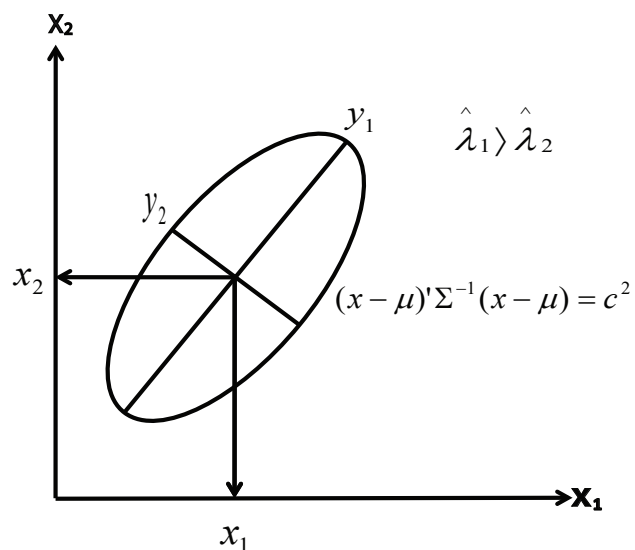
Figure 2.4: The image shows contour formation of the PCA distribution function when the eigenvalues are unequal.
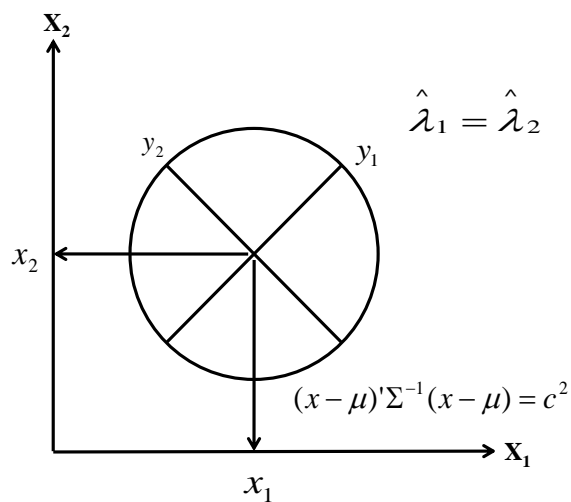
Figure 2.5: The image shows contour formation of the PCA distribution function when the eigenvalues are equal.

Chapter 3

Results and Discussion

3.1   Elemental Analysis

For each age group, two teeth samples were taken. Further, for each sample, the enamel and cementum parts were studied separately and 30 spectral data were generated for each segment. Therefore, for one age group, 120 LIBS spectra were generated. Altogether 720 raw spectral data were analyzed for this study, these data are evaluated with different approaches which will be discussed here in detail. The LIBS spectra of the enamel and cementum section in between the range of 200-1000 nm are recorded and shown in fig. 3.1.a. The LIBS spectra are taken from the age group of 30-40 years as it showed sharp emission lines compared to all other groups and is the average of 30 laser shots. We have further divided the LIBS spectra into two sections as shown in fig.3.1.b and fig.3.1.c. The former section shows elements between the range of 200-500 nm and the later section shows the elements from 580-1000 nm. The elements detected are identified with the
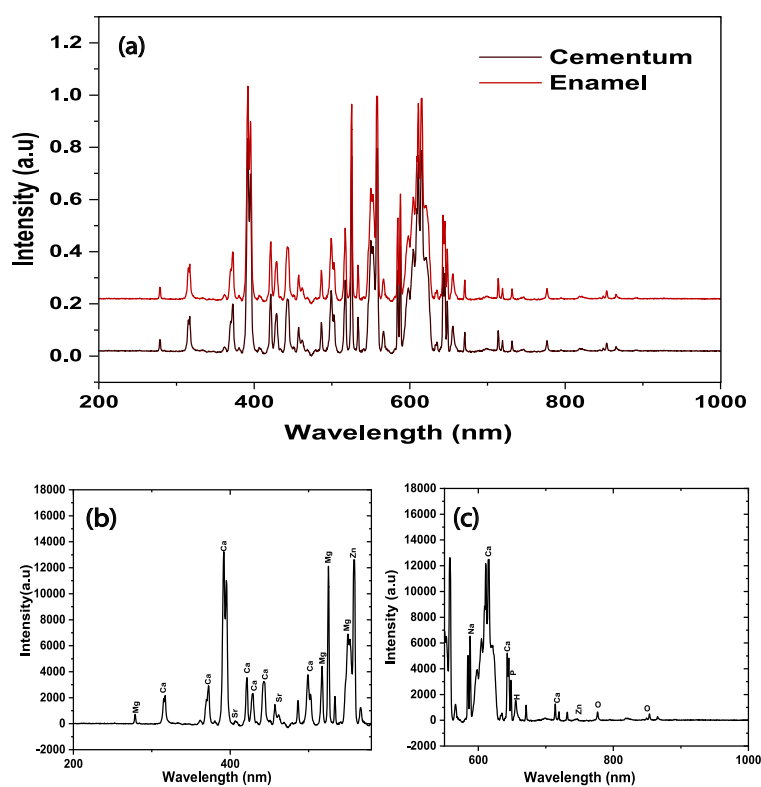
Figure 3.1: The figure represents LIBS spectra obtained for the teeth sample. Fig.(a) shows the spectra for the enamel and cementum sections of the teeth sample. Fig.(b) shows elements present in between wavelengths of 200-580 nm and fig.(c) shows the elements present in between wavelengths of 580-1000 nm of the sample.

National Institute of Standard and Technology (NIST)database are listed in table. 3.1 [124].

The basic tooth matrix of a crystalline enamel and cementum is a mineralized compound known as hydroxyapatite, with the following chemical formula $Ca_{10}(PO_4)_6(OH_2)$. Therefore, with reference to the literature it is observed that Ca is the most abundantly occurring element along with P, O, and H in the LIBS spectra of teeth samples. Apart from this, the signature of trace elements like Cl, F, Na, K, Sr, Mg, Mn, Cu, Zn, Pb are also obtained and found to be in conformity with the reported data in the literature [103, 104, 105, 106]. Of all the trace elements found in the teeth samples, Mg plays an important role in maintaining crystal stability. It is pointed out in the literature that Mg mineralizes the deciduous teeth in the early phase of its development and is later replaced by Ca after it is fully developed. Also, the deficiency of Ca due to decalcification occurring at the later stages is replaced by Mg, maintaining the crystal stability. Therefore, the concentration of Mg is recorded more in the enamel section. But in the case of cementum, the concentration of Ca is maintained as it is less exposed to dental infections causing decalcification of the crystal. Also, the Mg embedded during the development of the teeth samples is dissolved by the body fluids as they are rooted with the tissues. Due to these reasons, Mg concentrations are found to be less in the cementum section [122, 123, 133, 132]

With reference to the LIBS spectra obtained for our samples, the elements detected are listed in table3.1. The elements are detected for both the enamel and cementum sections but the intensity of the elements are found to vary. Sharp and abundant emission lines of Ca are observed along with the emission

Table 3.1: List of elements and their corresponding wavelengths recorded the LIBS spectra for enamel and cementum section of teeth samples.

Elements	Wavelengths
Ca	315.8 nm, 317.9 nm, 370.6 nm 393.3 nm, 422.6 nm, 428.3 nm, 442.5 nm, 458.5 nm, 500.1 nm, 610.2 nm, 714 nm, 720.2 nm, 849.8 nm, 854.2 nm
Mg	279.5 nm, 382.9 nm, 278.6 nm, 517.2 nm, 526.4 nm, 552.8 nm
Sr	407.7 nm, 460.7 nm
Na	588.9 nm, 615.4 nm
Zn	557.9 nm, 747.8 nm
P	643.6 nm, 649.6 nm
O	777.4 nm, 844.6 nm
H	656.3 nm

lines of P, H, and O which reflects the fact that these elements form the basic tooth matrix. The trace elements detected in our samples are Mg, Sr, Na, Zn. The variation in the intensity of elements is observed in the LIBS spectra of the sample with growing age and is illustrated in fig.3.2. The intensity of elements in the deciduous teeth and in the sample of age group beyond 50 years are found to be very less. Sharp emission lines of LIBS spectra are obtained for the samples of age above 20 years and less than 50 years. Also, from the fig.3.2, we can observe a difference in the emission lines of enamel and cementum. These differences in the LIBS spectra can be utilized to classify the teeth samples according to growing age which is the main motive of this study.
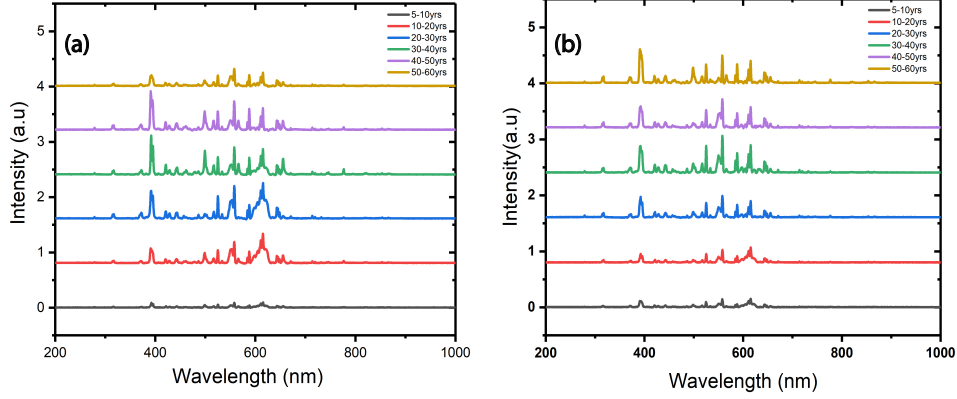
Figure 3.2: The figure illustrates the variation of LIBS spectra with ascending age groups for (a) cementum section and (b) enamel section.

3.2 Determination of plasma parameters

Optically thin plasma

The plasma plume so formed must be optically thin, or else the effect of self-absorption in sepctral lines will hinder the actual LIBS spectra. To verify this condition, the following relation must hold [119, 125].

$$\frac{I_{ki}}{I'_{ki}} = \frac{g_k A_{ki} \lambda'}{g'_k A^i_{ki} \lambda} \tag{3.1}$$

The intensity ratio of two interference-free emission lines I_{ki}, from a species having same upper energy level E_k must be comparable to the ratio obtained from the product of transition probability A_{ki} degeneracy factor g_k and the inverse wavelength λ of the respective emission lines. The subscripts in I_{ki}, represent upper and lower energy transition levels respectively. Intensity ratio for Ca and Mg emission lines, and the ratio obtained using their

corresponding A_{ki} and g_k taken from NIST database are listed in table 3.2. The approximate consistency between the two ratio values can be seen. This

Table 3.2: The ratio values for the intensity of interference free emission lines and their spectroscopic parameters are listed in the table which determines the condition for optically thin plasma.

Elements	$\frac{I_{ki}}{I'_{ki}}$	$\frac{g_k A_{ki} \lambda'}{g'_k A^i_{ki} \lambda}$
$Ca - I(443.635)/Ca - I(442.635)$	1.06	0.69
$Mg - I(517.169)/Mg - I(516.714)$	1.12	0.82

fulfills the condition for optically thin plasma.

Local thermodynamic equilibrium (LTE)

The plasma consists of electrons, atoms, ions, radiations and is the basis of LIBS. In thermal equilibrium, the population amongst atomic (and ionic) excited levels, ionization stages, translational states of electrons and heavy particles, as well as photon energy states can be described by Boltzmann distribution, Shah-Eggert equations, Maxwell and Planck distributions respectively all taken at the same temperature i.e,

$$T_{excitation} = T_{ionization} = T_{electron} = T_{heavyparticles} = T_{photondistribution} \quad (3.2)$$

Because of the escape of radiation from the plasma, the distribution of photon energies is always decoupled from the particles in the plasma. As a result the measured photon temperature $T_{photondistribution}$ is different from other temperatures. This leads to the establishment of a local thermodynamic equilibrium

(LTE) given by eq.3.3 [127, 128, 129]

$$T_{excitation} = T_{ionization} = T_{electron} = T_{heavyparticles} \neq T_{photondistribution} \quad (3.3)$$

Here, Saha-Boltzmann equations can be most conveniently used to determine the temperature of the plasma in LTE, as they hold for the number densities of the plasma constituents. It also implies the validity of the Maxwell distribution function for describing the energy of the electron and heavy particles. Also, these distributions adapt themselves to the local values of electron density and plasma temperature during the process of plasma expansion [128]. Therefore, to determine the plasma temperature in LTE, the intensity (I) of the emission lines, of n species in the plasma corresponding to a transition from upper energy level (E_k) to lower energy level (E_i), is given by Boltzmann population distribution function expressed as:

$$I_{ki}^n = \frac{hcN^n}{4\pi\lambda_{ki}} \frac{g_k A_{ki}}{U^n(T)} \exp^{-\frac{E_k^n}{K_B T}} \quad (3.4)$$

Here, I_{ki} is the intensity of a particular emission lines, λ_{ki} is the transition wavelength $g_k = 2J_k + 1$ and A_{ki} are the degeneracy factor/ satistical weight and transition probability for E_k respectively. The values of spectroscopic parameters are taken from NIST database. $U^n(T) = g_k \exp(\frac{-E_k}{K_B T})$ is the partition function, K_B is the Boltzmann constant. T is the plasma temperature and N^n is the electron number density of "n" species in plasma. The above

eq. 3.4 can be rewritten as:

$$\ln \frac{I_{ki}^{n} \lambda_{ki}}{g_k A_{ki}} = -\frac{E_k^n}{K_B T} + \ln \frac{hcN^n}{U^n(T)} \qquad (3.5)$$

known as the Boltzmann-Shah equation[126, 89, 92, 91], which represents a straight line whose slope is proportional to $-\frac{1}{K_B T}$ and the intercept is equal to $\ln \frac{hcN^n}{U^n(T)}$. The plasma temperature is determined by ploting $\ln \frac{I_{ki}^{n} \lambda_{ki}}{g_k A_{ki}}$ with E_k, taking the values from NIST database. The Boltzmann plot for the teeth samples are shown in fig.3.3. From the plot, we have taken the emission lines

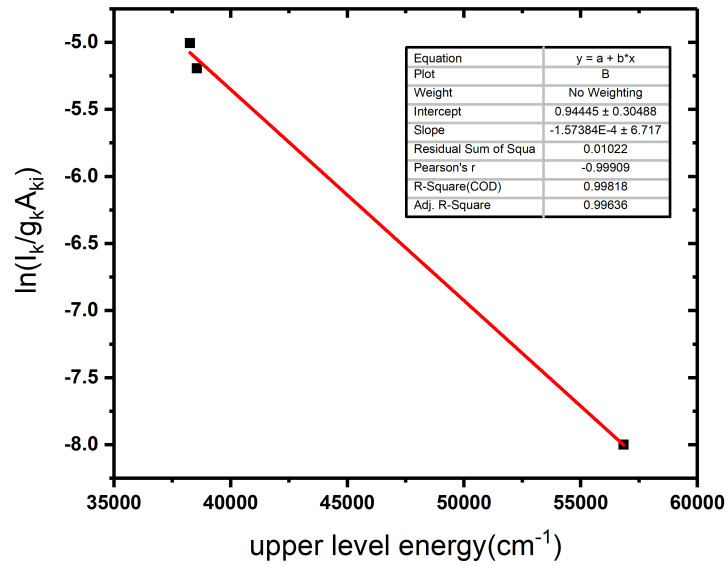Figure 3.3: The boltzmann plot for emission lines of Ca-I to determine the plasma temperature.

of Ca-I from the LIBS spectra of the cementum section recorded for the age group of 30-40 years. As mentioned before, the peaks observed in this group are more prominent compared to the other age groups. Also, Ca is the most abundantly found element in the sample and the process of decalcification is

less in the cementum section. From the plot, value of plasma temperature was found to be $6354.047 \pm 271.165K$

In order to validate the existance of LTE, minimum electron number density must be present in the plasma. Here, the collisional depopulation rate for all electronic levels of the atom be at least ten times larger than the radiative depopulation rate. In order to establish, we use the Mc Whirter condition. According to it the electron number density obtained using eq. 3.6 must be less than the experimentally measured (through stark broadening) electron number density obtained using eq. 3.7 [128, 127].

First, we estimate the electron number density with Mc Whirter condition, using eq. 3.6:

$$N_e(cm^{-3}) \geq 1.6 \times 10^{12}[T]^{1/2}[\triangle E]^3 \tag{3.6}$$

where, N_e is the electron density. Substituting the value of plasma temperature $T = 6354.047K$ and $\triangle E = 2.801eV$,obtained from the NIST database for Ca-I(442.67 nm), the value of N_e is found to be $3.05 \times 10^{15}cm^{-3}$.

Now, we experimentally evaluate the value of N_e with eq. 3.7

$$\mathrm{N_e} \approx (\frac{\triangle \lambda_{\mathrm{FWHM}}}{2\omega}) \times 10^{16}\mathrm{cm}^{-3} \tag{3.7}$$

where, $\triangle \lambda_{FWHM}$ are full width at half maxima value of the stark broadened profile and ω is impact factor. The emission line of Ca-I (442.67 nm) is taken and fitted with Lorentzian profile as shown in fig.3.4. The value of $\triangle \lambda_{FWHM}$ is found to be 4.17 nm. And, the value of ω for Ca-I at 442.67 nm lines for the plasma temperature between 5000-6000 K is found to be 0.286×10^{-1} [131]. Therefore, the value of electron density N_e is found to be $6.3135 \times 10^{17}cm^{-3}$.

The electron density obtained experimentally using eq. 3.7 is three order of

Model	Lorentz
Equation	y = y0 + (2*A/pi)*(w/(4*(x-xc)^2 + w^2))
Plot	B
y0	-159.31028 ± 41.42237
xc	442.67309 ± 0.07024
w	4.16776 ± 0.29389
A	13229.66819 ± 927.6529
Reduced Chi-S	16465.35656
R-Square(COD)	0.95854
Adj. R-Square	0.95518
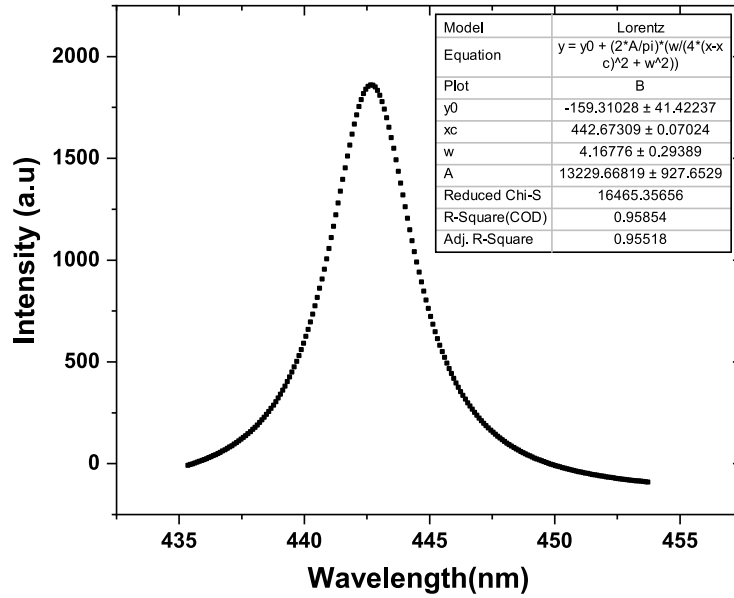
Figure 3.4: The figure shows Lorentzian fitted curve of CaI (442.67nm)to determine the FWHM of stark broadened profile.

magnitude higher in comparision to the value obtained using eq. 3.6. As mentioned, this fullfills the Mc Whirter criteria layout for LTE condition in our set-up.

3.3   Ratiometric Analysis

The motive of this work is to classify the teeth samples in different age groups using LIBS. For the classification, we have done the ratiometric analysis by taking the intensity ratios of $\frac{Ca-II}{Ca-I}$ and $\frac{Mg-II}{Mg-I}$. In the study of Abdel-Salam et al,[116, 117] to estimate the hardness of calcified tissue with LIBS, it is found that the value of repulsive force and the speed of shock wave generation by the ablated samples is more when the sample is hard. Therefore,

compared to soft samples ionization is more when a hard sample is ablated. Due to the difference in the ionization process, the ionic to neutral intensity ratio is proportional to the hardness of the sample and can be utilized to differentiate between hard and soft tissue. Firstly, they have measured the hardness of the enamel with a standard method and have compared it with hardness obtained by taking the ratio of ionic to neutral intensity lines of Ca and Mg, as they are elements occurring in abundance. The results were approximately the same proving that hardness obtained from $\frac{Ca-II}{Ca-I}$ and $\frac{Mg-II}{Mg-I}$ with LIBS, enables us to establish a qualitative comparison for a calcified tissue. Also, due to the high abundance of Ca, the effect of self-absorption is more compared to the minor elements are like Mg. Minor elements are optically thin and the effect of self-absorption is compensated by its low abundance. Therefore, better accuracy in the measurement of hardness is obtained from the ratio values of Mg.

Based on the above discussion to perform the ratiometric analysis emission lines of Ca-I(442.67 nm), Ca-II(422.70 nm), Ca-II(500.14 nm), Mg-I(517.16 nm), and Mg-II(526.43 nm) are taken for both the enamel and cementum section. Area given by $\frac{I_{ki}}{g_k A_{ki}}$, under each selected peak is obtained by the method of deconvolution. The spectroscopic parameters for the above emission lines are from the NIST database. Therefore, for the ratiometric analysis following ratios were monitored : $\frac{CaII(422.7nm)}{CaI(442.67nm)}, \frac{CaII(500.14nm)}{CaI(442.67nm)}, \frac{MgII(526.443nm)}{MgI(517.16nm)}$. Further in the thesis,the above three ratios are labelled as R1, R2, and R3 respectively. Based on these ratio values, firstly 1D classification is performed as a univariate analysis to gain a qualitative idea about the variation of these ratios with aging across the two sections of the sample. Secondly, a 2D clas-

sification is done to qualitatively classify the sample based on this hardness with age for both the section.

3.4 1D Classification

For the univariate classification of the samples using hardness, we choose a histogram plot. The mean and standard deviation values of R1, R2, and R3 were calculated for each of the enamel and cementum parts. Further, we discuss the outcome of the 1D classification.

Enamel

The mean value of 30 independent data and the standard deviation(SD) are listed in table 3.3 and shown as histogram in fig.3.5. The ratio values of R1, R2, and R3 are in the format of Mean $\pm$ SD. From fig.3.5 and table 3.3 it is observed that variation in R1 is negligible with the increasing age group. Whereas R2 calculated for the same element (peak appearing at a different wavelength) shows negligible variation till the age group of 50 years. For the age above 50 years, a drastic decrease in the value is observed. Enamel is the most mineralized and hardest section of a tooth and rich in Ca

Table 3.3: Calculation of ionic-to-neutral intensity ratio for different age groups of enamel section.

Ratio	5-10yrs	10-20yrs	20-30yrs	30-40yrs	40-50yrs	50-60yrs
R1	0.15$\pm$0.10	0.17$\pm$0.23	0.21$\pm$0.11	0.16$\pm$0.12	0.15$\pm$0.10	0.15$\pm$0.11
R2	2.23$\pm$0.78	1.78$\pm$0.62	2.10$\pm$0.74	1.98$\pm$1.53	2.49$\pm$0.64	1.09$\pm$0.74
R3	4.61$\pm$0.04	3.13$\pm$0.03	2.60$\pm$0.08	2.46$\pm$0.45	2.37$\pm$0.09	3.12$\pm$0.35

and Mg content. Studies suggest that the demineralization process occurs

only on the outer surface of the enamel. The deeper layer of the section remains mostly unaffected once the teeth develops[123, 132, 133]. As we are

Figure 3.5: The figure shows a histogram plot of the enamel section, where the variation of ratio intensities with age is illustrated.

examining the inner layer of the enamel, variation in the values of R1 and R2 is negligible with aging. The drop in R2 beyond the age of 50 years could occur due to calcium deficiency taking place with the growing age. Mg plays a major role in the regulation of hydroxyapatite, studies have found a higher content of Mg in caries infected teeth. Also, the deficient Ca ions due to various oral infections are replaced by Mg ions to maintain crystal stability. Therefore, in a few cases, the concentration of Mg increases with a decrease in the concentration of Ca [133]. As can be seen for R3, the value is maximum for 5-10 years and followed by the age- group of 50-60 years which

can be attributed to the above-mentioned scenario. Further, it is important to mention that these two age groups are in either the developing phase(5-10 years) or weakening phase (50-60 years) and hence, more likely to such changes.

Cementum

Secondly, we discuss the 1D classification for the cementum section of the samples. Here also, the mean value of 30 independent data and standard deviation (SD) are listed in table 3.4 and its corresponding histogram plot in fig.3.5. The values of R1, R2, and R3 are in the format of Mean ± SD. From the fig.3.5 and table 3.4 we observe negligible changes in the values of R1 but a significant variation in the values of R2 and R3. There is a significant growth in the values of R2 as it ascends across the minor to older age groups. Whereas, R3 has higher values for minor(5-20 years) age groups and it declines with the growing age (30-60 years).

Table 3.4: Calculation of ionic-to-neutral intensity ratio for different age groups of cementum section.

Ratio	5-10yrs	10-20yrs	20-30yrs	30-40yrs	40-50yrs	50-60yrs
R1	0.19±0.02	0.13±0.12	1.38±0.08	0.154±0.12	0.15±0.07	0.12±0.11
R2	0.15±0.50	3.37±0.15	1.56±0.12	4.231±0.46	4.26±0.45	2.83±0.12
R3	1.75±0.12	3.33±0.10	4.52±0.03	0.514±0.11	0.51±0.15	0.31±0.05

A deciduous (5-10 years) tooth has weak cementum as they are later replaced by mature ones. Therefore, fewer values for R1 and R2 were recorded indicating a less concentration of Ca during this premature phase of a tooth. With the lack of Ca, crystal stability is mainly maintained by Mg and hence, the value of R3 is more for this particular age group. Also, studies have found

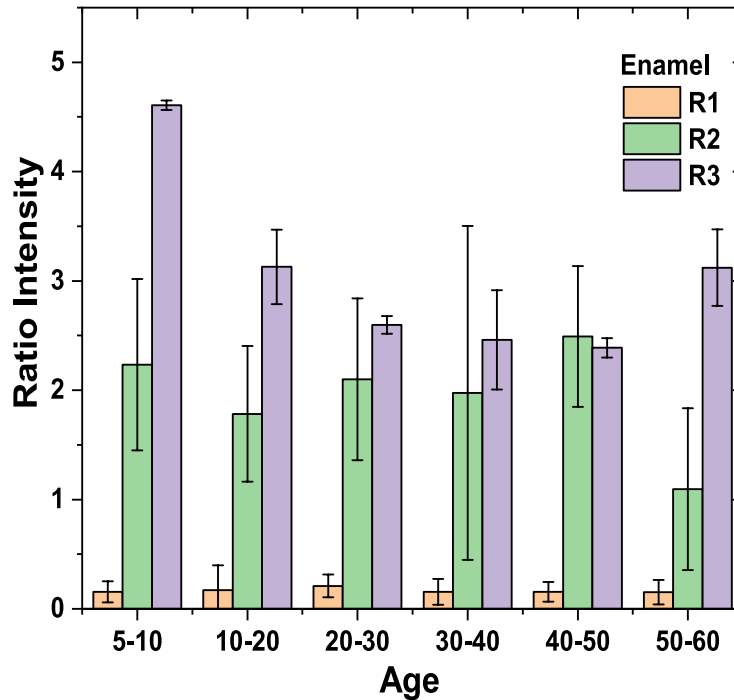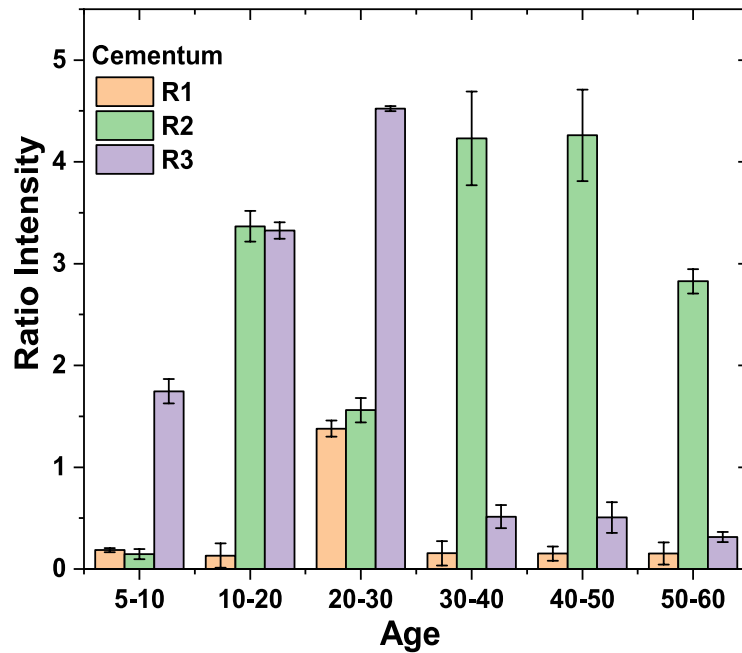Figure 3.6: The figure shows histogram plot of cementum section, where the variation of ratio intensities with age is illustrated.

that cementum is less exposed to caries infection and other dental amalgams. Therefore, the Ca present in the cementum after it is fully matured (20-60 years) remains preserved throughout the aging process. As the cementum is intact with the tissues and body fluids the Mg content in it is washed away as they are the trace elements and are unstable. This leads to the decrease in the concentration of Mg and so the value of R3 is found to decline for the cementum section with the growing age. The higher values of R2 indicate that Ca content is preserved and the cementum is healthy. We have observed an inconsistency from the regular pattern for the age group of 20-30 years. This could arise due to the influence of caries infection in the sample, as discussed earlier, these samples are clinically removed, and the influence of caries cannot be ruled out.

A comparative study of both the enamel and cementum section for each age group is shown in fig.3.7. From the profile, it is observed that in the age
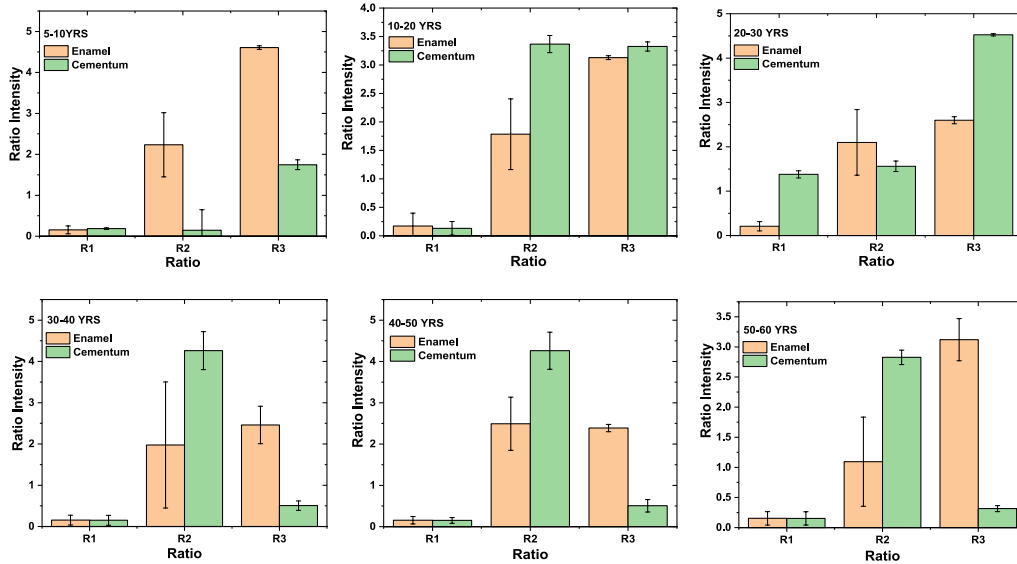
Figure 3.7: The figure shows a histogram plot for each age group to illustrate a comparative study for enamel and cementum part of the sample.

group of 5-10 years the enamel part is rich in mineral content compared to the cementum. This suggests that for a deciduous teeth, the enamel are stronger as compared to the cementum. With increasing age, the hardness of both the section has increased. From the age beyond 30 year it can be observed that the value of R2 decreases and R3 increases in the enamel section compared to the cementum section. As it is the exposed part of a tooth, with aging the Ca content of enamel tends to decrease and is replaced by Mg. Despite this, for a healthy teeth sample, the variation in enamel across the growing age is less compared to that of cementum as it is the most mineralized and hardest section of a human tooth.

Conclusion from 1D classification

Following conclusions can be drawn from 1D classification:

1. Enamel is the hardest and abundantly mineralized part of a human tooth. There exist minor variation in the values of R2 and R3 due to some clinical conditions, especially caries. In general, the variation of these ratios with growing age is not so prominent. Therefore, clarity of classification using the enamel section may not be as desired. The hardness values for the enamel section as estimated by Abdel-Salam et al, through the standard method shows that hardness observed with Ca lines is around 2.5 and 3.4 with Mg lines [116, 117]. Therefore, our findings are in confirmity with their results.

2. Remarkable changes in the values of R2 and R3 are recorded in the cementum section of the sample with ascending age. It shows that the hardness of the root section varies with aging. These changes are more prominent compared to the enamel section. Hence, a better classification may be obtained using the cementum section.

3. From the comparative study between the two sections it is found that with aging the enamel section is more vulnerable to changes in Ca content. In the enamel section, Ca deficiency cause due by various dental infections, and other factors are replaced by Mg ions. The cementum section is less exposed to such conditions, for this the Ca content of this section is preserved.

4. The value of R1 does not vary with aging and has no major contribution

to classification of the sample. This could arise due to the effect of self-absorption as Ca is the most abundantly occurring element. The difference in the wavelength values (422.7 nm and 442.65 nm) is not significant and similar intensities of both the wavelength are recorded. Therefore, rest of the analysis is carried out by taking the ratio values of R2 and R3.

5. The outcome of histogram profiles for both the section has given a rough outlet for the classification of human teeth with age. To further explore the results of 1D analysis for better clarity of classification, the 2D classification was next approached.

3.5 2D Classification

A comparative figure for the variations in ratio values with growing age and the possible causes are discussed in the above analysis, for both enamel and cementum sections. Now the 2D method will enable us to visualize a classification picture for the comparative analysis done so far. From the outcome of the 1D analysis, the ratio values of R2 and R3 are taken to perform 2D classification. The values of R2 along the X-axis and that of R3 along the Y-axis form the two variables for the 2D model.

Cementum

Firstly, we look into the cementum section, as more variations in the ratio values are recorded for this section. The 2D contour plot is shown in fig.3.8. The next important aspect of the 2D method is the euclidian distance (E.D)
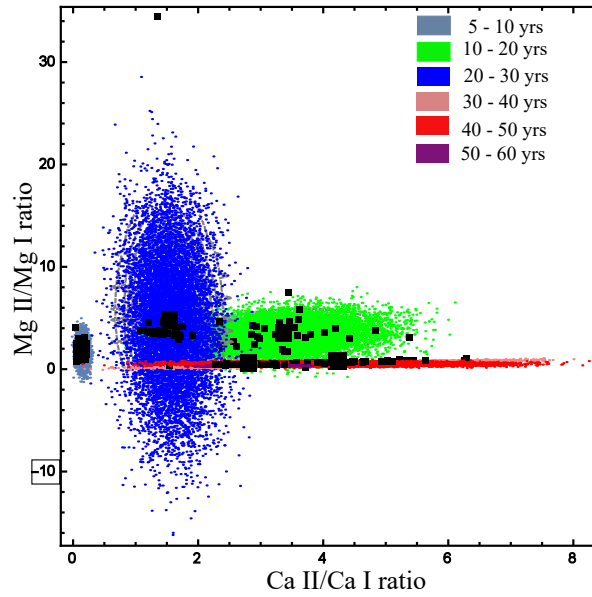
Figure 3.8: The figure represents 2D plot of R2 vs R3 for the cementum section.

calculated between the centers of one contour to another. Greater the distance better is the classification between two samples. From fig.3.8 we observe that contour for 10-20 years lies in the mean position concerning all other groups. Therefore, it is taken as a mean point to calculate E.D values to all other groups and the obtained values are listed in table3.5. From the

Table 3.5: Determination of euclidian distance from the center of age group 10-20 years to all other points for the cementum section with 2D model.

Euclidian distance	5-10 yrs	20-30 yrs	30-40 yrs	40-50 yrs	50-60 yrs
10-20 yrs to	3.61	2.24	2.96	2.98	3.10

fig.3.8 it is found that the contour of the first three age groups (5-10, 10-20, and 30-40 years) are distinct. Rest of the groups between 40-60 years are clustered together. This is because these three age groups have similar histogram profiles, with a small difference recorded for a group of 50-60 years.

The E.D as listed in table3.5 is observed highest for the group of 5-10 and 50-60 years, implying that the deciduous and mature teeth samples are classified. The age group of 30-40 and 40-50 years have similar values due to the similarity in their ratio values. Therefore, from the analysis, it is found that classification of human teeth based on the variation of hardness for different age grouped samples is possible by examining the cementum section.

Enamel

The 2D contour plot for the enamel section is shown in fig.3.9, we observe that the contours for all the age groups are clustered together. From the

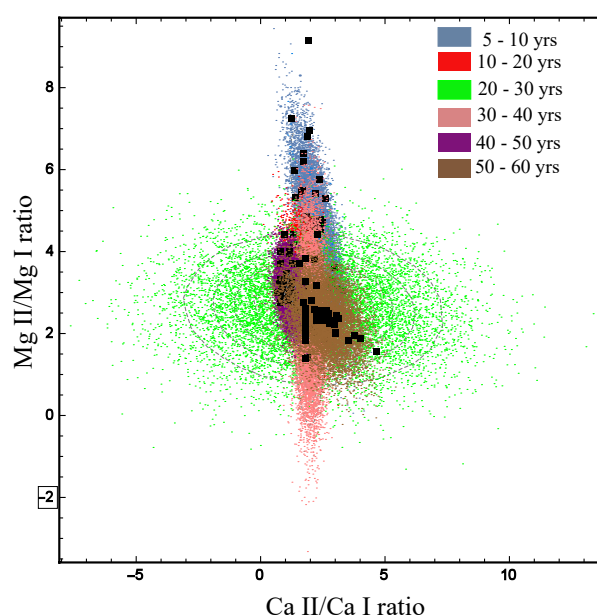Figure 3.9: The figure represents 2D plot of R2 vs R3 for the enamel section.

fig.3.9 we observe that contour for 20-30 years lies in the mean position concerning all other groups. Therefore, it is taken as a mean point to calculate E.D values to all other groups and the obtained values are listed in table 3.6.

In the 2D analysis of the enamel section, it is observed that the contour of

Table 3.6: Determination of euclidian distance from the center of age group 20-30 years to all other points for the enamel section with 2D model.

Euclidian distance	5-10 yrs	10-20 yrs	30-40 yrs	40-50 yrs	50-60 yrs
20-30 yrs	2.02	0.61	0.18	1.14	0.43

the samples is all clustered together. This is because a negligible variation in ratio values has been observed with growing age. Being the most mineralized section of a human tooth the variation in Ca and Mg are not significant. The decalcified part of the enamel due to caries is replaced by Mg therefore enamel section is always rich in mineral content. The E.D for enamel in table3.6 shows the highest value for the age group of 5-10 years. Therefore, this particular age group is classified from the rest of the group. The remaining groups have almost similar E.D values and hence a less possibility for classification. Henceforth, the classification of teeth with age considering the enamel part is not satisfactory like the one obtained from the cementum part.

From the analysis, it can be inferred that cementum can be a better choice to perform classification of sample based on the hardness. Enamel being the hardest section of a human sample, its hardness barely varies with aging. The drawback here is that for the cementum section too the classification is not clear for the age group between 40-60 years. Also, no specific inferences can be made for the enamel section. Therefore, to bring further clarity to the results, PCA is performed in the entire LIBS spectra.

3.6 PCA Classification

The analysis performed so far is based on the ratio values of Ca and Mg which represent the hardness of the sample. PCA is a multivariate analysis where it is possible to extend the sample measurements and its variables to multidimensions. Therefore, for this particular analysis, the entire LIBS spectra with a suitable background correction is analyzed. Here samples are arranged in the a form of matrix $(i \times j)$, where i rows are the number of observations or objects and j columns are the variables measured in the sample. Wavelengths between the range of 300-800 nm forms object or measurements and the intensity observed for various emission lines of the LIBS data form the variables of the sample matrix. A matrix of (1100×180) is formed for each of the enamel and cementum parts to perform the PCA.

Enamel

Firstly, let us discuss the PCA for enamel section of the sample. Let us first discuss the loading plot for the enamel section in fig.3.10. The loading plot of the PCA shows dependence of the variables and objects in the reduced sapce formed by the PC's. Next the score plot, helps to visualize the classification pattern of samples. The score plot of the enamel section is shown in fig.3.11, PC1 explains 88.7% and PC2 explains 4% of variation present in the data. From the loading plot in fig.3.10 it is observed that the intensity of elements is dependent on both PC1 and PC2. The intensity between the range of 500-600 nm is more towards PC2, these range mostly represents the emission lines of Mg. From 1D analysis it has been observed that for the enamel

Figure 3.10: The figure shows loading plot for enamel section, where the dependence of LIBS spectra on PC1 and PC2 is illustrated.

section, the decrease in Ca is replaced by Mg with growing age. Therefore, the emission lines of Mg are dependent on PC2. Emission lines of Ca along with the other minor elements are dependent on both PC1 and PC2. As the dependence of variables is seen in both the PCs, score plot in fig.3.11 is highly clustered together. There exist a high correlation between all the age groups of the samples. From the plot, it is observed that the age group of 5-10, 10-20, and 40-50 years have formed a distinct cluster. The rest of the age group (20-30, 30-40 and 50-60 years) has a scattered distribution. This result is in accordance to the fig.3.2, where it is observed that the intensity of infant age is less and it increases with aging. The intensity spectra remain almost the same for the age group of 20-30, 30-40 and 50-60 years. As the enamel
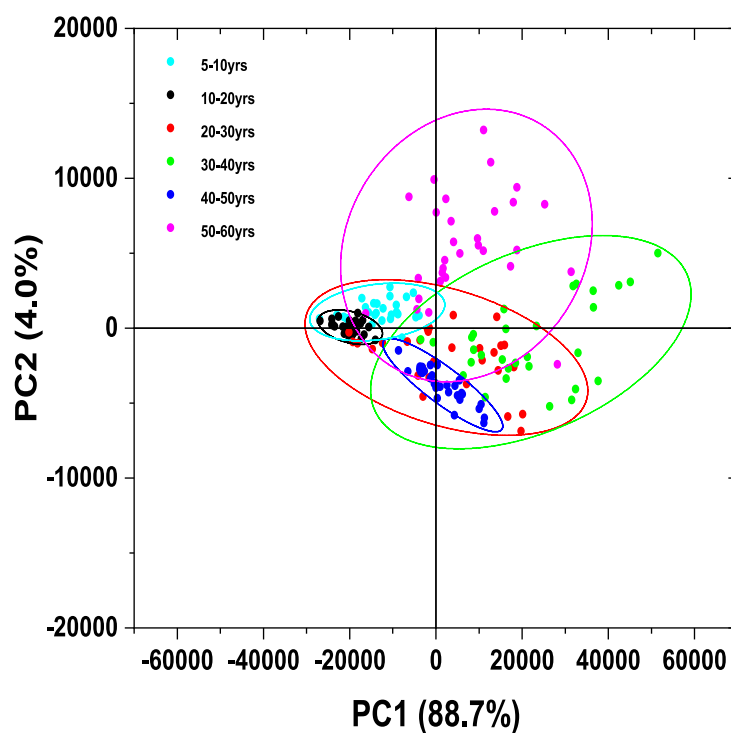
Figure 3.11: Score plot for enamel section.

section is highly mineralized, the intensity of elements does not vary much with aging. Though the Ca eroded due to various medical conditions are replaced by trace elements mainly Mg, still it remains rich with elements. For these reasons all the age groups are correlated to each other. A clear classification of the sample concerning different age groups is not clear by examining the enamel section of the sample.

Cementum

Secondly, let us discuss the loading plot of the cementum section, in fig.3.12. From the plot, it is observed that the majority of elements are dependent on PC1. Elements between the range of 600-650 nm, which mainly represent the

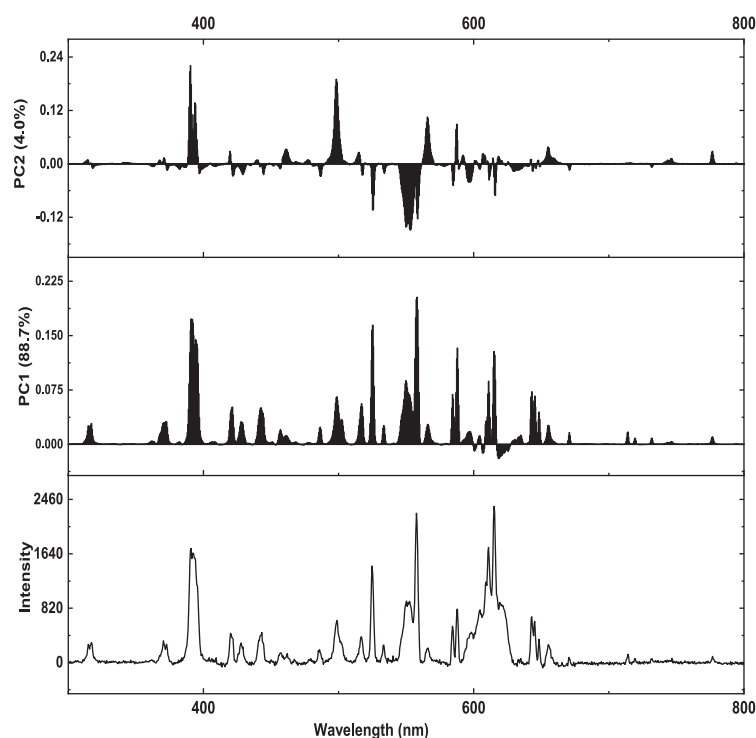emission lines of Ca and are more towards PC2. We observe such features
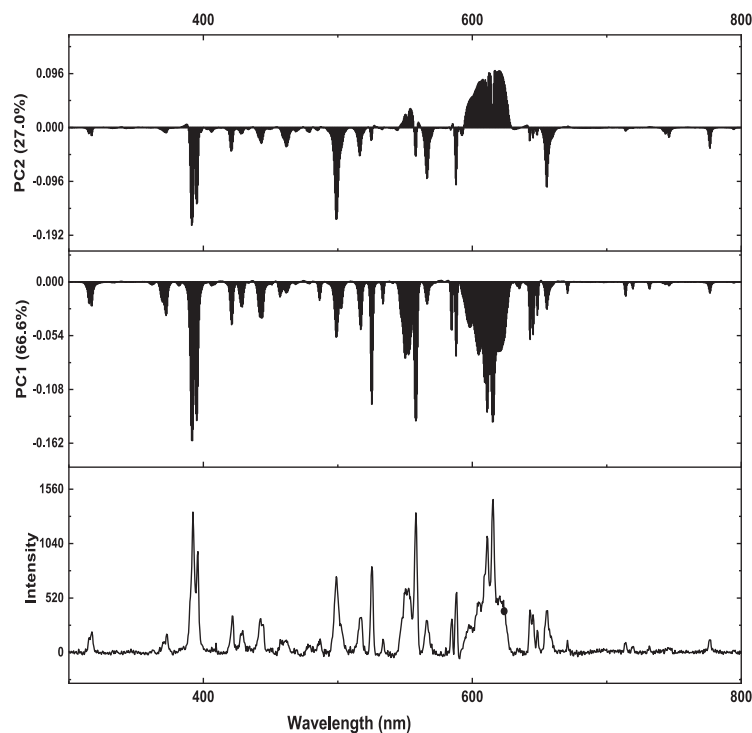
Figure 3.12: The figure shows loading plot for cementum section, where the dependence of LIBS spectra on PC1 and PC2 is illustrated.

in the loading plot of the cementum because they are less exposed to the various dental infection and has less amount of trace elements. This is in accordance with the results obtained in the 1D analysis. The Ca present in the individual sample is preserved but it is found to vary with age. This variation in the Ca with aging is reflected in the loading plot of the PCA. Now let us examine the score plot of the cementum illustrated fig.3.13. PC1 explains 66.6% and PC2 explains 27.0% of the varaince present in data. From the plot, it is observed that the sample of 5-10 and 50-60 years are correlated and its variance is explained mostly by PC1. The sample in the age of 5-
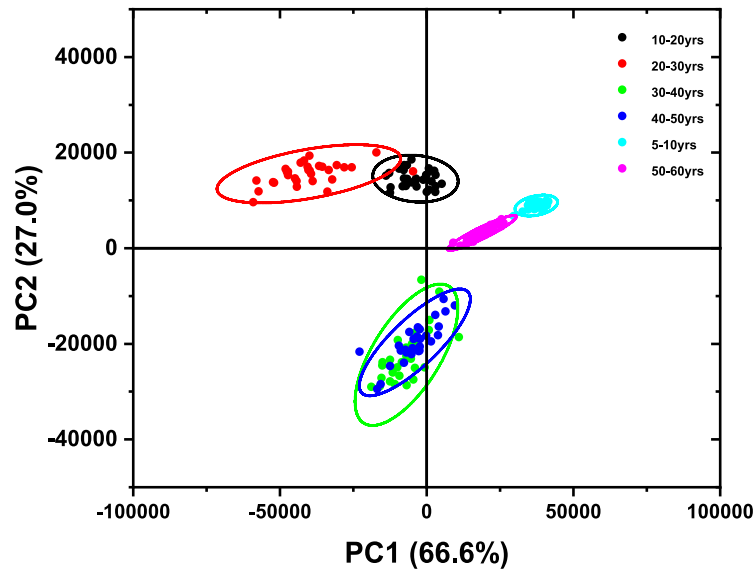
Figure 3.13: Score plot for cementum section.

10 years is deciduous teeth which eventually gets replaced and have weak intensity spectra. Again at the age of 50-60 years, the root section becomes weak due to various dental infections and a deficit of minerals. Therefore, there is a resemblance in the intensity spectra of the two age groups and are correlated as they both fall in the positive region of PC1. The clusters are still clearly distinguishable from one another. Sample in the age of 10-20 and 20-30 years are correlated and lies in the PC2 region. At this phase, the sample is replaced by the permanent teeth and in the developing phase. From intensity spectra of the cementum in fig.3.2, a small difference in the intensity between the two age groups is observed. For this, a correlation exists between the age group but again they are distinguishable from each other. A strong correlation between the age group of 30-40 and 40-50 is seen and is dependent on both PCs. At this stage, the sample is fully developed and has strong cementum. Also, the intensity spectra for this particular

age group are sharp and similar compared to all other age groups. Hence, they are clustered together and but are classified from the rest of the sample. PCA testifies that the cementum section is suitable to classify a human teeth sample with varying ages.

Chapter 4

Conclusion and Future prospects

4.1 Conclusion

Here we summarize the results that we have obtained from each of our analysis:

1. Firstly, with LIBS we have efficiently performed the rapid elemental analysis of human teeth samples of various age groups. The identification of major tooth matrix as well as trace elements could be performed which are in accordance with the literature.

2. Estimation of all the plasma parameters are performed and it shows the abundance of Ca is more compared to Mg, which are our major focused elements for determination of hardness of the tissue.

3. After fulfilling all the criteria for ratiometric calculations, the hardness

of tissue is monitored by observing its variation with ascending age for enamel and cementum section.

4. The 1D classification provided us a quantitative picture of how hardness varies with age for the enamel and cementum section independently. Enamel though subjected to various dental infections, its mineral is retained and the hardness barely varies with age. The hardness of cementum is prone to changes with age, initially, it is weak and slowly the hardness increases with age till the age of 30-50 years but eventually falls as a person ages. Again, we observe from the comparative study of enamel and cementum that even for the same age group the there is a difference in the two sections and enamel is stronger compared to cementum.

5. Mg plays a major role in regulating the tooth matrix. The Ca that gets demineralized with caries is mainly replaced by Mg and it maintains the hardness of the teeth. Also, as Mg is less abundant hardness can be more accurately estimated by it. Due to the effect of self absorption, the nearby emission lines of Ca cannot give the required results as we observed it in the ratio value R1. But it is not the case with Mg the nearby emission lines can give equally good results.

6. The quantitative picture that has been generated so far is brought into the picture with 2D classification. It shows that better classification is obtained for cementum compared to enamel. This aids ratiometric and 1D results but still, little clarity was required to obtain better classification results.

7. The variation in LIBS spectra that was observed in the ascending age group could be brought into the picture with PCA. A clear clarification could be made as the contribution of each emission line to classify the samples could be learned. The classification was better projected and it confirmed the results obtained with all the above approaches. We could finally confirm that the cementum section of the human teeth sample is better suited to perform the age-wise classification of teeth compared to the enamel.

Therefore, we come to a conclusion that the classification of human teeth with ascending age can be better performed with the cementum section of a human tooth. The variation in hardness and intensity spectra of the sample in various age groups is more vividly observed in this section and has been testified with 1D, 2D, and PCA analysis. The enamel section comparatively is found to vary less when the hardness and intensity spectra with ascending age are concerned. The enamel section is more likely to be affected by several dental infections and environmental conditions. Therefore, there persists a fluctuation in the Ca and Mg values when hardness is concerned. In spite of this, the abundance of elements in this section does not decline with aging. Hence, its classification with the aging factor is not clear. Therefore, LIBS of the cementum section is the better fit in order to analyze the difference and classify human teeth over the range of various age groups. The efficiency of LIBS to perform elemental analysis of a calcified biological sample is supported by this work and many others present in the literature. Of the three different methods applied to analyze the sample, PCA is better suited to study LIBS data as it can efficiently handle the LIBS data relating to all the

information. A clear profile of classification for both the section projected with LIBS which fulfills our main objective.

4.2   Future prospects

The samples collected for the work were limited because the medical history, environmental conditions of the person was not documented. The classification can be further improved by incorporating the parameters, arising because of the medical backgrounds. Also, classification can be improvised with the introduction of supervised chemometric techniques like PLS-DA, SIMCA, and many more. The LTE conditions can be improved by introducing the time delay between the plasma formation and capturing the emission lines. The classification of teeth samples with age can serve a useful purpose in the field of forensic, archeology, and odontology. Therefore, it can be further pursued to construct a robust system with LIBS in combination with multivariate analysis.

Bibliography

[1] Welz, B., and Sperling,M. Atomic absorption spectrometry. *John Wiley & Sons*, 2008.

[2] Fortes, F. J., Moros, J., Lucena, P., Cabaln, L. M., & Laserna, J. J. Laser-induced breakdown spectroscopy. *Analytical chemistry*,85(2): 640-669, 2013.

[3] L. Radziemski, D. Cremers. A brief history of laser-induced breakdown spectroscopy: from the concept of atoms to LIBS 2012. *Spectrochimica Acta Part B: Atomic Spectroscopy*, 87: 3-10, 2013.

[4] Gbor. Galbcs. A critical review of recent progress in analytical laser-induced breakdown spectroscopy. *Analytical and bioanalytical chemistry*, 407(25): 7537-7562, 2015

[5] V.K. Singh, V. Kumar, J. Sharma, Y. Khajuria, K. Kumar. Importance of laser induced breakdown spectroscopy for biomedical applications: a comprehensive review. *Materials Focus*, 3(3):169-182, 2014.

[6] S.C. Jantzi, V. Motto-Ros, F. Trichard, Y. Markushin, N. Melikechi, A. De Giacomo. Sample treatment and preparation for laser-induced breakdown spectroscopy. Spectrochimica Acta Part B: Atomic Spectroscopy, 115: 52-63, 2016.

[7] Bro, Rasmus, and Age K. Smilde. Principal component analysis. Analytical Methods, 6(9): 2812-2831, 2014

[8] Shlens, Jonathon. A tutorial on principal component analysis. arXiv preprint, arXiv:1404.1100, 2014

[9] H. Addi, J. Williams Lynne. Principal component analysis. Wiley Interdisciplinary Reviews: Comput-ational Statistics, 2(4): 433-459, 2010

[10] Pozka, Pavel, et al. On the utilization of principal component analysis in laser-induced breakdown spectroscopy data analysis, a review. Spectrochimica Acta Part B: Atomic Spectroscopy, 148: 65-82, 2018

[11] Kumar, R., & Sharma, V. Chemometrics in forensic science. *TrAC Trends in Analytical Chemistry*, 105:191-201, 2018.

[12] Pathak, A. K., Singh, A., Kumar, R., & Rai, A. K. Laser-induced breakdown spectroscopy coupled with PCA study of human tooth. *National Academy Science Letters*, 42(1):87-90, 2019.

[13] Singh, V. K., Kumar, V., & Sharma, J. (2015). Importance of laser-induced breakdown spectroscopy for hard tissues (bone, teeth) and other calcified tissue materials. *Lasers in medical science*, 30(6):1763-1778, 2015.

[14] Singh, V. K., and Rai, A. K. Prospects for laser-induced breakdown spectroscopy for biomedical applications: a review. *Lasers in medical science*, 26(5): 673-687, 2011.

[15] Perez-Jordan, M. Y., Salvador, A., De la Guardia, M. Determination of Sr, K, Mg And Na In Human Teeth by Atomic Spectrometry Using a Microwave-Assisted Digestion in a Closed Flow System. *Analytical letters*, 31(5):867-877, 1998.

[16] Spvkov, V., md,J. Determination of lead in teeth of children for monitoring purposes by electrothermal atomic absorption spectrometry. *Spectrochimica Acta Part B: Atomic Spectroscopy*, 54(5): 865-871, 1999.

[17] Winefordner, J. D., Gornushkin, I. B., Correll, T., Gibb, E., Smith, B. W., Omenetto, N. Comparing several atomic spectrometric methods to the super stars: special emphasis on laser induced breakdown spectrometry, LIBS, a future super star. *Journal of Analytical Atomic Spectrometry*, 19(9):1061-1083, 2004.

[18] Becker, J. S., Matusch, A., & Wu, B. Bioimaging mass spectrometry of trace elementsrecent advance and applications of LA-ICP-MS: A review. Analytica chimica acta, 835:1-18, 2014.

[19] Cox, A., Keenan, F., Cooke, M., & Appleton, J. Trace element profiling of dental tissues using laser ablation-inductively coupled plasma-mass spectrometry. *Fresenius' journal of analytical chemistry*, 354(2):254-258, 1996.

[20] Bridge, C. M., Powell, J., Steele, K. L., & Sigman, M. E. Forensic comparative glass analysis by laser-induced breakdown spectroscopy. *Spectrochimica Acta Part B: Atomic Spectroscopy*, 62(12):1419-1425, 2007.

[21] Meissner, K., Lippert, T., Wokaun, A.,& Guenther, D. Analysis of trace metals in comparison of laser-induced breakdown spectroscopy with LA-ICP-MS. *Thin Solid Films*, 453:316-322, 2004.

[22] de Carvalho, G. G. A., Guerra, M. B. B., Adame, A., Nomura, C. S., Oliveira, P. V., de Carvalho, H. W. P., ... & Krug, F. J. Recent advances in LIBS and XRF for the analysis of plants. *Journal of Analytical Atomic Spectrometry*, 33(6): 919-944, 2018.

[23] Almirall, J. R., Umpierrez, S., Castro, W., Gornushkin, I., & Wineford-ner, J. Forensic elemental analysis of materials by laser induced break-down spectroscopy (LIBS). *International Society for Optics and Photonics*, 5778:657-666, 2005 .

[24] Naes, B. E., Umpierrez, S., Ryland, S., Barnett, C., & Almirall, J. R. A comparison of laser ablation inductively coupled plasma mass spectrome-try, micro X-ray fluorescence spectroscopy, and laser induced breakdown spectroscopy for the discrimination of automotive glass. *Spectrochimica Acta Part B: Atomic Spectroscopy*, 63(10):1145-1150, 2008.

[25] Kumar, N., Bansal, A., Sarma, G. S., and Rawal, R. K. Chemometrics tools used in analytical chemistry: An overview. *Talanta*, 123:186-199, 2014.

[26] Myakalwar, A. K., Sreedhar, S., Barman, I., Dingari, N. C., Rao, S. V., Kiran, P. P., and Kumar, G. M. Laser-induced breakdown spectroscopy-based investigation and classification of pharmaceutical tablets using mul-tivariate chemometric analysis. *Talanta*, 87:53-59, 2011.

[27] Tiwari, P. K., Awasthi, S., Kumar, R., Anand, R. K., Rai, P. K., and Rai, A. K. Rapid analysis of pharmaceutical drugs using LIBS coupled with multivariate analysis. *Lasers in Medical Science*, 33(2):263-270, 2018.

[28] Tiwari, P. K., Rai, P. K., and Rai, A. K. Applications of LIBS in drug analysis. *In Laser-Induced Breakdown Spectroscopy.Elsevier*, (pp. 311-328),2020.

[29] Doucet, F. R., Faustino, P. J., Sabsabi, M., Lyon, R. C. Quantita-tive molecular analysis with molecular bands emission using laser-induced breakdown spectroscopy and chemometrics. *Journal of Analytical Atomic Spectrometry*, 23(5):694-701, 2008.

[30] de Carvalho, G. G. A., Nunes, L. C., de Souza, P. F., Krug, F. J., Alegre, T. C., Santos Jr, D. Evaluation of laser induced breakdown spectrome-try for the determination of macro and micronutrients in pharmaceutical tablets. *Journal of analytical atomic spectrometry*,25(6):803-809, 2010.

[31] Wang, J., Liao, X., Zheng, P., Xue, S., Peng, R. Classification of Chi-nese herbal medicine by laser-induced breakdown spectroscopy with prin-cipal component analysis and artificial neural network. *Analytical letters*, 51(4):575-586, 2018.

[32] Wang, J., Shi, M., Zheng, P., Xue, S. Quantitative analysis of lead in tea samples by laser-induced breakdown spectroscopy. *Journal of Applied Spectroscopy*,84(1):188-193, 2017.

[33] Wang, J., Zheng, P., Liu, H.,& Fang, L. Classification of Chinese tea leaves using laser-induced breakdown spectroscopy combined with the discriminant analysis method. *Analytical Methods*, 8(15):3204-3209, 2016.

[34] Wang, J., Li, X., Zheng, P., Zheng, S., Mao, X., Zhao, H., & Liu, R. Characterization of the Chinese traditional medicine Artemisia annua by laser-induced breakdown spectroscopy (LIBS) with 532 nm and 1064 nm excitation. *Analytical Letters*, 53(6):922-936, 2020.

[35] Tripathi, D. K., Pathak, A. K., Chauhan, D. K., Dubey, N. K., Rai, A. K., & Prasad, R. An efficient approach of laser induced breakdown spectroscopy (LIBS) and ICAP-AES to detect the elemental profile of Ocimum L. species. *Biocatalysis and Agricultural Biotechnology*, 4(4):471-479, 2015.

[36] Liu, X., Zhang, Q., Wu, Z., Shi, X., Zhao, N.,& Qiao, Y. Rapid elemental analysis and provenance study of Blumea balsamifera DC using laser-induced breakdown spectroscopy. *Sensors*, 15(1):642-655,2015.

[37] Kim, G., Kwak, J., Kim, K. R., Lee, H., Kim, K. W., Yang, H., & Park, K. Rapid detection of soils contaminated with heavy metals and oils by laser induced breakdown spectroscopy (LIBS). *Journal of Hazardous Materials*, 263:754-760, 2013.

[38] Chatterjee, S., Singh, M., Biswal, B. P., Sinha, U. K., Patbhaje, S., & Sarkar, A. Application of laser-induced breakdown spectroscopy (LIBS) coupled with PCA for rapid classification of soil samples in geothermal areas. *Analytical and bioanalytical chemistry*,411(13):2855-2866,2019.

[39] Lewis, D. E., Martinez, J., Akpovo, C. A., Johnson, L., Chauhan, A., & Edington, M. D. Discrimination of bacteria from Jamaican bauxite soils using laser-induced breakdown spectroscopy. *Analytical and bioanalytical chemistry*, 401(7):2225, 2011.

[40] Sirven, J. B., Salle, B., Mauchien, P., Lacour, J. L., Maurice, S., & Manhes, G. Feasibility study of rock identification at the surface of Mars by remote laser-induced breakdown spectroscopy and three chemometric methods. *Journal of Analytical Atomic Spectrometry*, 22(12):1471-1480, 2007.

[41] Clegg, S. M., Sklute, E., Dyar, M. D., Barefield, J. E., & Wiens, R. C. Multivariate analysis of remote laser-induced breakdown spectroscopy spectra using partial least squares, principal component analysis, and related techniques. *Spectrochimica Acta Part B: Atomic Spectroscopy*, 64(1):79-88, 2009.

[42] Lanza, N. L., Clegg, S. M., Wiens, R. C., McInroy, R. E., Newsom, H. E., & Deans, M. D. Examining natural rock varnish and weathering rinds with laser-induced breakdown spectroscopy for application to ChemCam on Mars. *Applied Optics*, 51(7):B74-B82, 2012.

[43] Pozka, P., Demidov, A., Kaiser, J., Keivanian, J., Gornushkin, I., Panne, U., & Riedel, J. Laser-induced breakdown spectroscopy for in situ qualitative and quantitative analysis of mineral ores. *Spectrochimica Acta Part B: Atomic Spectroscopy*, 101:155-163, 2014.

[44] Gottfried, J. L., Harmon, R. S., De Lucia Jr, F. C., & Miziolek, A. W. Multivariate analysis of laser-induced breakdown spectroscopy chemical signatures for geomaterial classification. *Spectrochimica Acta Part B: Atomic Spectroscopy*, 64(10):1009-1019, 2009.

[45] Death, D. L., Cunningham, A. P., & Pollard, L. J. Multi-element and mineralogical analysis of mineral ores using laser induced breakdown spectroscopy and chemometric analysis. *Spectrochimica Acta Part B: Atomic Spectroscopy*, 64(10):1048-1058, 2009.

[46] Harmon, R. S., Russo, R. E., & Hark, R. R. Applications of laser-induced breakdown spectroscopy for geochemical and environmental analysis: A comprehensive review. *Spectrochimica Acta Part B: Atomic Spectroscopy*, 87:11-26, 2013.

[47] Yao, M., Lin, J., Liu, M., & Xu, Y. Detection of chromium in wastewater from refuse incineration power plant near Poyang Lake by laser induced breakdown spectroscopy. *Applied Optics*, 51(10):1552-1557, 2012.

[48] Youli, Y., Weidong, Z., Huiguo, Q., Xuejiao, S. U., & Ke, R. E. N. Simultaneous determination of trace lead and chromium in water using laser-induced breakdown spectroscopy and paper substrate. *Plasma Science and Technology*,16(7):683, 2014.

[49] Haider, A. F. M. Y., Ullah, M. H., Khan, Z. H., Kabir, F., & Abedin, K. M. Detection of trace amount of arsenic in groundwater by laser-induced breakdown spectroscopy and adsorption. *Optics & Laser Technology*, 56:299-303, 2014.

[50] Markiewicz-Keszycka, M., Cama-Moncunill, X., Casado-Gavalda, M. P., Dixit, Y., Cama-Moncunill, R., Cullen, P. J., & Sullivan, C. Laser-induced breakdown spectroscopy (LIBS) for food analysis: A review. *Trends in Food Science & Technology*, 65:80-93, 2017.

[51] Senesi, G. S., Cabral, J., Menegatti, C. R., Marangoni, B., & Nicolodelli, G. Recent advances and future trends in LIBS applications to agricultural materials and their food derivatives: An overview of developments in the last decade (20102019). Part II. Crop plants and their food derivatives. *TrAC Trends in Analytical Chemistry*, 118:453-469, 2019.

[52] Senesi, G. S., Romano, R. A., Marangoni, B. S., Nicolodelli, G., Villas-Boas, P. R., Benites, V. M., & Milori, D. M. B. P. Laser-induced breakdown spectroscopy associated with multivariate analysis applied to discriminate fertilizers of different nature. *Journal of Applied Spectroscopy*, 84(5):923-928, 2017.

[53] Liu, X., Feng, X., Liu, F., Peng, J., & He, Y. Rapid identification of genetically modified maize using laser-induced breakdown spectroscopy. *Food and Bioprocess Technology*, 12(2):347-357, 2019.

[54] Moncayo, S., Manzoor, S., Rosales, J. D., Anzano, J., & Caceres, J. O. Qualitative and quantitative analysis of milk for the detection of adulteration by Laser Induced Breakdown Spectroscopy (LIBS). *Food chemistry*, 232:322-328, 2017.

[55] Velioglu, H. M., Sezer, B., Bilge, G., Baytur, S. E., & Boyaci, I. H. Identification of offal adulteration in beef by laser induced breakdown spectroscopy (LIBS). *Meat science*, 138:28-33, 2018.

[56] Hanasil, N. S., Raja Ibrahim, R. K., Duralim, M., Sapingi, H. H. J., & Mahdi, M. A. EXPRESS: Signal Enhancement Evaluation of Laser Induced Breakdown Spectroscopy of Extracted Animal Fats Using a Principal Component Analysis Approach. *Applied Spectroscopy*, 0003702820915532, 2020.

[57] Capuano, E., Van der Veer, G., Boerrigter-Eenling, R., Elgersma, A., Rademaker, J., Sterian, A., & Van Ruth, S. M. Verification of fresh grass feeding, pasture grazing and organic farming by cows farm milk fatty acid profile. *Food Chemistry*, 164:234-241, 2014.

[58] Goode, S. R., Morgan, S. L., Hoskins, R., & Oxsher, A. Identifying alloys by laser-induced breakdown spectroscopy with a time-resolved high resolution echelle spectrometer *Journal of Analytical Atomic Spectrometry*, 15(9):1133-1138, 2000.

[59] Zhang, T., Yan, C., Qi, J., Tang, H., & Li, H. Classification and discrimination of coal ash by laser-induced breakdown spectroscopy (LIBS) coupled with advanced chemometric methods. *Journal of Analytical Atomic Spectrometry*, 32(10):1960-1965, 2017.

[60] Horsfall, J. P., Trivedi, D., Smith, N. T., Martin, P. A., Coffey, P., Tournier, S., ... & Law, G. T. A new analysis workflow for discrimination of nuclear grade graphite using laser-induced breakdown spectroscopy. *Journal of environmental radioactivity*, 199:45-57, 2019.

[61] Ruan, F., Zhang, T., & Li, H. Laser-induced breakdown spectroscopy in archeological science: a review of its application and future perspectives. *Applied Spectroscopy Reviews*, 54(7):573-601, 2019.

[62] Colao, F., Fantoni, R., Ortiz, P., Vazquez, M. A., Martin, J. M., Ortiz, R., & Idris, N. Quarry identification of historical building materials by means of laser induced breakdown spectroscopy, X-ray fluorescence and chemometric analysis. *Spectrochimica Acta Part B: Atomic Spectroscopy*, 65(8):688-694, 2010.

[63] Awasthi, S., Kumar, R., Rai, G. K., & Rai, A. K. Study of archaeological coins of different dynasties using libs coupled with multivariate analysis. *Optics and Lasers in Engineering*, 79:29-38, 2016.

[64] Zhou, T., & Peng, Y. Kernel principal component analysis-based Gaussian process regression modelling for high-dimensional reliability analysis. *Computers & Structures*, 241:106358, 2020.

[65] Ince, H., & Trafalis, T. B. Kernel principal component analysis and support vector machines for stock price prediction. *Iie Transactions*, 39(6):629-637, 2007.

[66] He, J., Liu, Y., Pan, C., & Du, X. Identifying Ancient Ceramics Using Laser-Induced Breakdown Spectroscopy Combined with a Back Propagation Neural Network. *Applied Spectroscopy*, 73(10):1201-1207, 2019.

[67] Kumar, R., & Sharma, V. Chemometrics in forensic science. *TrAC Trends in Analytical Chemistry*, 105:191-201, 2018.

[68] Rinke-Kneapler, C.N., & Sigman, M.E Applications of laser spectroscopy in forensic science. *Laser Spectroscopy for Sensing: Woodhead Publishing*, 461 - 495, 2014.

[69] Balah, A., Fekry, O., & Aied Taha Nassef, O. A Further Analysis of Laser Induced Breakdown Spectroscopy Ink Pens Spectra Using Principal Component Analysis (PCA) for Forensic Characterization. *Arab Journal of Nuclear Sciences and Applications*, 52(2):72-78, 2019.

[70] Jantzi, S. C., & Almirall, J. R. Characterization and forensic analysis of soil samples using laser-induced breakdown spectroscopy (LIBS). *Analytical and bioanalytical chemistry*, 400(10):3341-3351, 2011.

[71] Rodriguez-Celis, E. M., Gornushkin, I. B., Heitmann, U. M., Almirall, J. R., Smith, B. W., Winefordner, J. D., & Omenetto, N. Laser induced breakdown spectroscopy as a tool for discrimination of glass for forensic applications. *Analytical and bioanalytical chemistry*, 391(5):1961, 2008.

[72] Munson, C. A., De Lucia Jr, F. C., Piehler, T., McNesby, K. L., & Miziolek, A. W. Investigation of statistics strategies for improving the discriminating power of laser-induced breakdown spectroscopy for chemical and biological warfare agent simulants. *Spectrochimica Acta Part B: Atomic Spectroscopy*, 60(7-8):1217-1224, 2005.

[73] Liu, K., Tian, D., Li, C., Li, Y., Yang, G., & Ding, Y. A review of laser-induced breakdown spectroscopy for plastic analysis. *TrAC Trends in Analytical Chemistry*, 110:327-334, 2019.

[74] Unnikrishnan, V. K., Choudhari, K. S., Kulkarni, S. D., Nayak, R., Kartha, V. B., & Santhosh, C. Analytical predictive capabilities of laser induced breakdown spectroscopy (LIBS) with principal component analysis (PCA) for plastic classification. *Rsc Advances*, 3(48):25872-25880, 2013.

[75] Costa, V. C., Aquino, F. W. B., Paranhos, C. M., & Pereira-Filho, E. R. Identification and classification of polymer e-waste using laser-induced breakdown spectroscopy (LIBS) and chemometric tools. *Polymer Testing*, 59:390-395, 2017.

[76] Aguirre, M. ., Hidalgo, M., Canals, A., Nbrega, J. A., & Pereira-Filho, E. R. Analysis of waste electrical and electronic equipment (WEEE) using laser induced breakdown spectroscopy (LIBS) and multivariate analysis. *Talanta*, 117:419-424, 2013.

[77] Gottfried, J. L., De Lucia, F. C., Munson, C. A., & Miziolek, A. W. Laser-induced breakdown spectroscopy for detection of explosives residues: a review of recent advances, challenges, and future prospects. *Analytical and bioanalytical chemistry*, 395(2):283-300, 2009.

[78] Shaik, A. K., Epuru, N. R., Syed, H., Byram, C., & Soma, V. R. Femtosecond laser induced breakdown spectroscopy based standoff detection of explosives and discrimination using principal component analysis. *Optics express*, 26(7):8069-8083, 2018.

[79] Lazic, V., Palucci, A., Jovicevic, S., Poggi, C., & Buono, E. Analysis of explosive and other organic residues by laser induced breakdown spectroscopy. *Spectrochimica Acta Part B: Atomic Spectroscopy*, 64(10):1028-1039, 2009.

[80] Lazic, V., Palucci, A., Jovicevic, S., & Carpanese, M. Detection of explosives in traces by laser induced breakdown spectroscopy: Differences from organic interferents and conditions for a correct classification. *Spectrochimica Acta Part B: Atomic Spectroscopy*, 66(8):644-655, 2011.

[81] Gaudiuso, R., Melikechi, N., Abdel-Salam, Z. A., Harith, M. A., Palleschi, V., Motto-Ros, V., & Busser, B. Laser-induced breakdown spectroscopy for human and animal health: A review. *Spectrochimica Acta Part B: Atomic Spectroscopy*, 152:123-148, 2019.

[82] Wang, Q., Xiangli, W., Teng, G., Cui, X.,& Wei, K. A brief review of laser-induced breakdown spectroscopy for human and animal soft tissues: pathological diagnosis and physiological detection. *Applied Spectroscopy Reviews*, 1-21, 2020.

[83] Ghasemi, F., Parvin, P., Reif, J., Abachi, S., Mohebbifar, M. R., & Razzaghi, M. R. Laser induced breakdown spectroscopy for the diagnosis of several malignant tissue samples. *Journal of Laser Applications*, 29(4):042005, 2017.

[84] Wang, J., Li, L., Yang, P., Chen, Y., Zhu, Y., Tong, M., ... & Li, X. Identification of cervical cancer using laser-induced breakdown spectroscopy coupled with principal component analysis and support vector machine. *Lasers in medical science*, 33(6):1381-1386, 2018.

[85] El-Hussein, A., Kassem, A. K., Ismail, H., & Harith, M. A. Exploiting LIBS as a spectrochemical analytical technique in diagnosis of some types of human malignancies. *Talanta*, 82(2):495-501, 2010.

[86] Han, J. H., Moon, Y., Lee, J. J., Choi, S., Kim, Y. C., & Jeong, S. Differentiation of cutaneous melanoma from surrounding skin using laser-induced breakdown spectroscopy. *Biomedical optics express*, 7(1):57-66, 2016.

[87] Teran-Hinojosa, E., Sobral, H., Snchez-Prez, C., Prez-Garca, A., Alemn-Garca, N., & Hernndez-Ruiz, J. Differentiation of fibrotic liver tissue using laser-induced breakdown spectroscopy. *Biomedical optics express*, 8(8):3816-3827, 2017.

[88] Yueh, F. Y., Zheng, H., Singh, J. P., & Burgess, S. Preliminary evaluation of laser-induced breakdown spectroscopy for tissue classification. *Spectrochimica Acta Part B: Atomic Spectroscopy*, 64(10):1059-1067, 2009.

[89] Singh, V. K., Singh, V., Rai, A. K., Thakur, S. N., Rai, P. K., & Singh, J. P. Quantitative analysis of gallstones using laser-induced breakdown spectroscopy. *Applied Optics*, 47(31): G38-G47, 2008.

[90] Pathak, A. K., Singh, V. K., Rai, N. K., Rai, A. K., Rai, P. K., Rai, P. K., ... & Baruah, G. D. Study of different concentric rings inside gallstones with LIBS. *Lasers in medical science*, 26(4):531-537, 2011.

[91] Pathak, A. K., Kumar, R., Singh, V. K., Agrawal, R., Rai, S., & Rai, A. K. Assessment of LIBS for spectrochemical analysis: a review. *Applied Spectroscopy Reviews*, 47(1):14-40, 2012.

[92] Singh, V. K., Rai, A. K., Rai, P. K., & Jindal, P. K. Cross-sectional study of kidney stones by laser-induced breakdown spectroscopy. *Lasers in medical science*, 24(5):749-759, 2009.

[93] Khalil, A. A. I., Gondal, M. A., Shemis, M., & Khan, I. S. Detection of carcinogenic metals in kidney stones using ultraviolet laser-induced breakdown spectroscopy. *Applied Optics*, 54(8):2123-2131, 2015.

[94] Fang, X., Ahmad, S. R., Mayo, M.,& Iqbal, S. Elemental analysis of urinary calculi by laser induced plasma spectroscopy. *Lasers in Medical Science*, 20(3-4):132-137, 2005.

[95] Jaswal, B. B. S., & Singh, V. K. Analytical assessments of gallstones and urinary stones: a comprehensive review of the development from laser to LIBS. *Applied Spectroscopy Reviews*, 50(6):473-498, 2015.

[96] Anzano, J., & Lasheras, R. J. Strategies for the identification of urinary calculus by laser induced breakdown spectroscopy. *Talanta*, 79(2):352-360, 2009.

[97] Hamzaoui, S., Khleifia, R., Jadane, N., & Lakhdar, Z. B. Quantitative analysis of pathological nails using laser-induced breakdown spectroscopy (LIBS) technique. *Lasers in Medical Science*, 26(1):79-83, 2011.

[98] Hosseinimakarem, Z., & Tavassoli, S. H. Analysis of human nails by laser-induced breakdown spectroscopy. *Journal of Biomedical Optics*, 16(5):057002, 2011.

[99] Abdel-Salam, Z. A., Palleschi, V., & Harith, M. A. Study of the feeding effect on recent and ancient bovine bones by nanoparticle-enhanced laser-induced breakdown spectroscopy and chemometrics. *Journal of advanced research*, 17:65-72, 2019.

[100] Mehari, F., Rohde, M., Knipfer, C., Kanawade, R., Klmpfl, F., Adler, W., ... & Schmidt, M. Laser induced breakdown spectroscopy for bone and cartilage differentiation-ex vivo study as a prospect for a laser surgery feedback mechanism. *Biomedical optics express*, 5(11): 4013-4023, 2014.

[101] Pretty, I. A., & Sweet, D. A look at forensic dentistryPart 1: The role of teeth in the determination of human identity., *British dental journal*, 190(7):359-366, 2001.

[102] Higgins, D., & Austin, J. J. Teeth as a source of DNA for forensic identification of human remains: a review. *Science & Justice*, 53(4):433-441, 2013.

[103] R. K. Thareja, A. K. Sharma, S. Shukla. Spectroscopic investigations of carious tooth decay. *Medical engineering and physics*, 30(9): 1143-1148, 2008.

[104] A. Khalid, S. Bashir, M. Akram, Q. S. Ahmed. The variation in surface morphology and hardness of human deciduous teeth samples after laser irradiation. *Laser Physics*, 27(11):115-601, 2017.

[105] V. K. Singh, A. K. Rai. Potential of laser-induced breakdown spectroscopy for the rapid identification of carious teeth. *Lasers in medical science*, 26(3): 307-315, 2011.

[106] R. Z. LeGeros, A. Ito, K.Ishikawa, T. Sakae, J. P. LeGeros. Fundamentals of hydroxyapatite and related calcium phosphates. Advanced Biomaterials: Fundamentals, Processing, and Applications, 19-52, 2009.

[107] M. H. Niemz. Laser-tissue interactions. Springer-Verlag Berlin Heidelberg, 78-79, 2007.

[108] O. Samek, D. C. S. Beddows, H. H. Telle, G. W. Morris, M. Liska, J. Kaiser. Quantitative analysis of trace metal accumulation in teeth using laser-induced breakdown spectroscopy. Applied Physics A, 69(1): S179-S182, 1999.

[109] Samek, O., Lika, M., Kaiser, J., Beddows, D. C. S., Telle, H. H., & Kukhlevsky, S. V. Clinical application of laser-induced breakdown spectroscopy to the analysis of teeth and dental materials. *Journal of clinical laser medicine & surgery*, 18(6):281-289, 2000.

[110] Samek, O., Telle, H. H., & Beddows, D. C. *Laser-induced breakdown spectroscopy: a tool for real-time, in vitro and in vivo identification of carious teeth. BMC Oral Health*, 1(1):1, 2001.

[111] Gazmeh, M., Bahreini, M., & Tavassoli, S. H. Discrimination of healthy and carious teeth using laser-induced breakdown spectroscopy and partial least square discriminant analysis. *Applied optics*, 54(1):123-131, 2015.

[112] Fortes, F. J., Perez-Carceles, M. D., Sibon, A., Luna, A., & Laserna, J. J. Spatial distribution analysis of strontium in human teeth by laser-induced breakdown spectroscopy: application to diagnosis of seawater drowning. *International journal of legal medicine*, 129(4):807-813, 2015.

[113] Moncayo, S., Manzoor, S., Ugidos, T., Navarro-Villoslada, F., & Caceres, J. O. Discrimination of human bodies from bones and teeth remains by laser induced breakdown spectroscopy and neural networks. *Spectrochimica Acta Part B: Atomic Spectroscopy*, 101:21-25, 2014.

[114] W. Tawfik, S. El-Tayeb. Human enamel in ancient (34001085 BC) and recent Egypt. Science Echoes, 7: 28-38, 2006.

[115] A. M. Alhasmi, M. A. Gondal, M. M. Nasr, S. Shafik, Y. B. Habibullah. Detection of toxic elements using laser-induced breakdown spectroscopy in smokers and nonsmokers teeth and investigation of periodontal parameters. Applied optics, 54(24): 7342-7349, 2015.

[116] Abdel-Salam, Z. A., Galmed, A. H., Tognoni, E., & Harith, M. A. Estimation of calcified tissues hardness via calcium and magnesium ionic to atomic line intensity ratio in laser induced breakdown spectra. *Spectrochimica Acta Part B: Atomic Spectroscopy*, 62(12):1343-1347, 2007.

[117] Abdel-Salam, Z. A., Nanjing, Z., Anglos, D., & Harith, M. A. Effect of experimental conditions on surface hardness measurements of calcified tissues via LIBS. *Applied physics B*, 94(1):141-147, 2009.

[118] Galiov, M., Kaiser, J., Fortes, F. J., Novotn, K., Malina, R., Proke, L., ... & Kanick, V. Multielemental analysis of prehistoric animal teeth by laser-induced breakdown spectroscopy and laser ablation inductively coupled plasma mass spectrometry. Applied Optics, 49(13):C191-C199, 2010.

[119] Sreedhar, Sunku, Manoj Kumar Gundawar, and S. Venugopal Rao. Laser Induced Breakdown Spectroscopy for Classification of High Energy Materials using Elemental Intensity Ratios. Defence Science Journal, 64.4,(2014).

[120] Johnson, Richard Arnold, and Dean W. Wichern. Applied multivariate statistical analysis. *Upper Saddle River, NJ: Prentice hall*, (Vol.5,No.8,), 2002

[121] Pozka, P., Klus, J., Hrdlika, A., Vrbel, J., karkov, P., Prochazka, D., ... & Kaiser, J. Impact of laser-induced breakdown spectroscopy data normalization on multivariate classification accuracy. *Journal of Analytical Atomic Spectrometry*, 32(2):277-288,2017.

[122] T. M. Nakata, R. J. Stepnick, I. Zipkin. Chemistry of human dental cementum: the effect of age and fluoride exposure on the concentration of ash, fluoride, calcium, phosphorus and magnesium. *Journal of periodontology*, 43(2), 115-124, 1972.

[123] K. A. Selvig, S. K. Selvig. Mineral content of human and seal cementum. *Journal of dental research*, 41(3), 624-632, 1962.

[124] NIST National Institute of Standards and Technology USA electronic database

[125] R. E. Russo, X. L. Mao, J. Yoo, J. J. Gonzalez Laser ablation. *In Laser-induced breakdown spectroscopy*, Elsevier: 41-70, 2007.

[126] Barthlemy, O., Margot, J., Laville, S., Vidal, F., Chaker, M., Le Drogoff, B., ... & Sabsabi, M. Investigation of the state of local thermodynamic equilibrium of a laser-produced aluminum plasma. Applied spectroscopy, 59(4) : 529-536,2005.

[127] Cristoforetti, G., Tognoni, E., & Gizzi, L. A. Thermodynamic equilibrium states in laser-induced plasmas: from the general case to laser-induced breakdown spectroscopy plasmas. Spectrochimica Acta Part B: Atomic Spectroscopy, 90, 1-22, 2013.

[128] Cristoforetti, G., De Giacomo, A., Dell'Aglio, M., Legnaioli, S., Tognoni, E., Palleschi, V., & Omenetto, N. Local thermodynamic equilibrium in laser-induced breakdown spectroscopy: beyond the McWhirter criterion. Spectrochimica Acta Part B: Atomic Spectroscopy, 65(1), 86-95, 2010.

[129] Capitelli, M., Capitelli, F., & Eletskii, A. Non-equilibrium and equilibrium problems in laser-induced plasmas. Spectrochimica Acta Part B: Atomic Spectroscopy, 55(6), 559-574, 2000.

[130] R.McWhirter. Spectral intensities, Plasma Diagnostic Techniques, 201, 1965.

[131] N.Konjevi, A. Lesage, J. Fuhr, W.Wiese. Experimental Stark widths and shifts for spectral lines of neutral and ionized atoms (a critical review of selected data for the period 1989 through 2000). Journal of Physical and Chemical Reference Data,31(3): 819-927, 2002.

[132] J. de Dios Teruel, A. Alcolea, A. Hernndez, A. J. O. Ruiz. Comparison of chemical composition of enamel and dentine in human, bovine, porcine and ovine teeth. *Archives of oral biology*, 60(5):768-775, 2015.

[133] E.Klimuszko, K.Orywal, T.Sierpinska, ,J. Sidun, M. Golebiewska. Evaluation of calcium and magnesium contents in tooth enamel without any pathological changes: in vitro preliminary study. *Odontology*,106(4): 369-376, 2018.
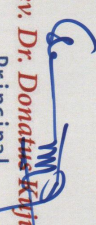
International Seminar on

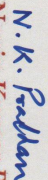## Correlative Advancement on Analytical and Applied Physics

Organized by

Department of Physics in collaboration with IQAC St.Joseph's College,

Northpoint, Darjeeling

Date: October 21-22, 2019

Venue: St. Joseph's ,College Darjeeling

Certified that Prof./Dr./Mr./Ms. _Puja Pradhan_

of _Department of Physics, Sikkim University_ has delivered the

Keynote Address/ an Invited Talk/ presented a paper entitled _Classification_

With Using laser Induced Breakdown Spectroscopy / partici-

pated in the International Seminar on Correlative Advancement on Analytical

and Applied Physics.

Fr. Rev. Dr. Donatus Kujur, S.J
Principal
St. Joseph's College, Darjeeling

N.K. Pradhan
Dr. Navin Kumar Pradhan
Co-ordinator

Debarghya Goswami
Convenor